Synthetic Biology: A Unifying View and Review Using Analog Circuits

Jonathan J. Y. Teo, Sung Sik Woo, *Student Member, IEEE*, and Rahul Sarpeshkar

***Abstract*—We review the field of synthetic biology from an analog circuits and analog computation perspective, focusing on circuits that have been built in living cells. This perspective is well suited to pictorially, symbolically, and quantitatively representing the nonlinear, dynamic, and stochastic (noisy) ordinary and partial differential equations that rigorously describe the molecular circuits of synthetic biology. This perspective enables us to construct a canonical analog circuit schematic that helps unify and review the operation of many fundamental circuits that have been built in synthetic biology at the DNA, RNA, protein, and small-molecule levels over nearly two decades. We review 17 circuits in the literature as particular examples of feedforward and feedback analog circuits that arise from special topological cases of the canonical analog circuit schematic. Digital circuit operation of these circuits represents a special case of saturated analog circuit behavior and is automatically incorporated as well. Many issues that have prevented synthetic biology from scaling are naturally represented in analog circuit schematics. Furthermore, the deep similarity between the Boltzmann thermodynamic equations that describe noisy electronic current flow in subthreshold transistors and noisy molecular flux in biochemical reactions has helped map analog circuit motifs in electronics to analog circuit motifs in cells and vice versa via a 'cytomorphic' approach. Thus, a body of knowledge in analog electronic circuit design, analysis, simulation, and implementation may also be useful in the robust and efficient design of molecular circuits in synthetic biology, helping it to scale to more complex circuits in the future.**

***Index Terms*—Analog circuits, biological circuit design, cellular engineering, cytomorphic, feedback, resource consumption, review, synthetic biology analog computation.**

I. Introduction

THOUGH we now know a lot about the parts list of cells, we have been unable to engineer cells to get these parts to work together in more complex circuits: After nearly two decades of research, the largest circuit built within a cell is still a synthetic '6-logic-gate circuit' [1]. A state-of-the-art '12-part circuit' necessitated 4 kinds of cells with 3 logic gates within each [2]. In contrast, Nature herself has designed complex nonlinear, stochastic, analog circuits within cells that have over 30 000 state variables [3]–[5]; her circuits comprise asynchronous feedback circuits in pathways significantly more complex than feed-forward, high-molecular-copy-number logic gates. Furthermore, her circuits are so energy, part-count, and molecular-copy-number efficient that her computational efficiency per operation is 4 to 5 orders of magnitude more efficient than man-made systems in nanoscale GHz electronic processes and is already near the thermodynamic limits of physics [3], [6]. To develop complex circuits that are as robust and as efficient as in nature, we will need to address 5 main challenges:

1) **Oversimplified Design Paradigms and Abstractions**: Even though molecules are discrete and digital, cells do not operate with reliable '1' and '0' signals like modern-day computers do. Rather, the signals in cells are inherently probabilistic as all thermodynamic signals are. In the typical copy numbers seen in cells, many such probabilistic Poisson events combine to create a mean 2–5 bit-precise analog signal with noise [4]; RNA signals are significantly more noisy and probabilistic than protein signals that have the benefit of more averaging. The basic building-block DNA, RNA, and protein circuits of cells are not logic gates but are described by analog reaction-network differential and stochastic (probabilistic or noisy) differential equations. The signals can be thresholded above a certain molecular count to yield a '1' and thresholded below a certain molecular count to yield a '0' if only the saturated portion of basis functions are utilized (as in Fig. 1, adapted from [7]). But the transfer function is not really a logic gate and does not compose neatly like logic gates do. Most logical on/off ratios in biological circuits are in the 10–100 range such that 'switches' in these logic circuits are about 4 to 10 orders of magnitude more leaky than most switches in digital computers today. In certain cases, truly discrete state transitions caused by positive feedback do cause absolute digital behavior, e.g., in the differentiation or division of a cell or in cell-cycle transitions [5]; but, digital circuits are a special case of analog circuits that already represent saturated behavior. As in engineering, analog circuit motifs that are a quantitatively accurate and insightful representation of the actual underlying differential equations but that are not oversimplified are essential for design.
2) **Non-Modular Behavior and Loading**: Downstream pathways in cells consume molecules and therefore affect

Manuscript received February 17, 2015; revised May 13, 2015; accepted July 13, 2015. Date of publication September 11, 2015; date of current version September 22, 2015. This work was supported in part by grants from the National Science Foundation under CCF 1124247 and CCF 1348519 and in part by a grant from the Semiconductor Research Corporation under Proposal P16730. This paper was recommended by Associate Editor S. Wong.

J. J. Y. Teo and S. S. Woo are with the Research Laboratory of Electronics, Massachusetts Institute of Technology, Cambridge, MA 02139 USA.

R. Sarpeshkar is with the Research Laboratory of Electronics, Massachusetts Institute of Technology, Cambridge, MA 02139 USA, and also with the Departments of Engineering, Microbiology & Immunology, Physics, and Physiology & Neurobiology, Dartmouth College, Hanover, NH 03755 USA (e-mail: rahul.sarpeshkar@dartmouth.edu).

Color versions of one or more of the figures in this paper are available online at http://ieeexplore.ieee.org.

Digital Object Identifier 10.1109/TBCAS.2015.2461446

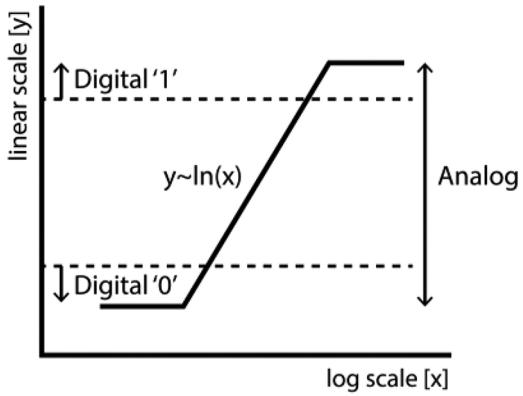

Fig. 1. [7]. Digital circuits are a special case of analog circuits.

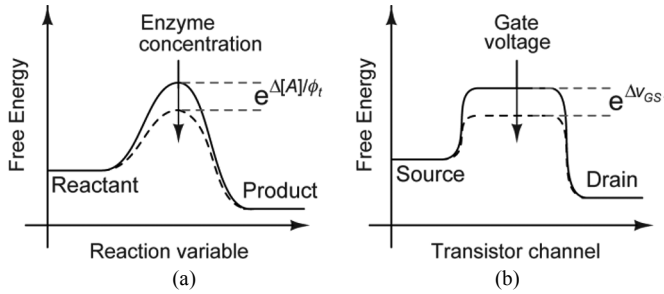

Fig. 2. Cytomorphic mapping [3]. (a) Free energy change of a typical chemical reaction along its reaction coordinate. (b) Free energy change of an electron moving in a transistor in the subthreshold regime.

the functions of upstream ones, which may no longer be abstracted to have the same function [8]. Therefore circuits in cells frequently exhibit non-modularity and 'loading' and do not behave like simple, modular, clean, well-defined digital logic gates but as complex stochastic analog feedback loops and circuits that are always subject to loading and interaction between modules [3], [9]. Pathway 'cross talk' [10] drastically affects modularity in logic gates, and less so in softer analog circuits where failure is less catastrophic.

3) **Metabolic Loading and Molecular Toxicity**: The rate of energy consumption within most cells is constrained to have a total power budget near 10 M ATP/sec [3]–[5], [11], [12], in part to avoid excessive Reactive Oxygen Species (ROS) generation. Energy-efficient cells likely outcompeted other cells in early evolution as well [13]. If cells are engineered to synthetically produce molecules at high copy numbers to ensure reliable deterministic function, metabolic loading can quickly result [4], [13]–[15]. For example, just building a 10-bit-precise deterministic synthetic digital genetic adder in yeast takes 163 logic gates and would consume its entire power budget even with generous assumptions [4]! Furthermore, high molecular counts increase osmolarity and cross reactivity and are toxic to cells. It is no surprise that engineering complex circuits within cells without paying careful attention to molecular counts and metabolic loading [14], [15] has not scaled in nearly two decades.
4) **Resource Consumption of Cellular Machinery**: There are a finite number of polymerases, ribosomes, RNAases, and proteases within a cell. The use of shared cellular machinery by synthetic circuits can and does have an impact on the natural functions of the cell. For example, producing proteins on one plasmid can affect protein production on another plasmid or in the cell [14]–[17]. Recent work has shown that proteases are shared [16] and can cause wanted [18] (also see Fig. 10) and unwanted coupling in circuits. Therefore, it is essential to design and analyze cells with a paradigm that accounts for such consumption. The availability of these resources affect the operation of synthetic circuits in different host environments, contexts, and media [10], [15].
5) **Stochastics**: Molecular copy numbers in cells are necessarily constrained such that many cellular signals operate with 2-to-5 bit precision [4], [19] and are effectively noisy analog signals rather than deterministic digital ones.However, simulating and designing for stochastics is incredibly computationally intensive, taking hours for even 6-state-variable Poisson Gillespie simulations [20]–[22]. It has been estimated that it would take several years for genome-scale stochastic Poisson simulation of a single cell cycle in a bacterium [23]. Even highly approximate, non-Poisson and largely deterministic simulations of a single cell cycle of the smallest bacterium on earth with 528 genes took 10 hours on a 128-node LINUX cluster [24]. Bacterial persister cells and tumor cells become resistant to drugs because of rare cells whose stochastics enables them to survive and reproduce later [25], [26]. The copy number of important molecules like *p53* [5], which regulates cell death, and whose expression is mutated in more than half of all cancers, corresponds to very low molecular concentrations and high stochasticity. Stochastics and molecular copy number are essential in evaluating the efficiency, information capacity, resource consumption, toxicity, and robustness of any engineered cellular circuit and are fundamental to biology. Yet, they are often treated as an afterthought rather than being incorporated into design from the word go.

A rational and principled approach to biological design may be possible via a 'cytomorphic' mapping shown in Fig. 2 [3]: *There is a deep connection between 'electronics', which is about the controlled, relatively long-range motions of electrons between devices, and 'chemistry', which is about the controlled, relatively short-range motions of electrons between atoms and molecules*. Fig. 2 shows that there are striking similarities between chemical reaction dynamics and electronic current flow in the sub-threshold regime of transistor operation: Electron concentration at the source is analogous to reactant concentration; electron concentration at the drain is analogous to product concentration; forward and reverse current flows in the transistor are analogous to forward and reverse reaction rates in a chemical reaction; the forward and reverse currents in a transistor are exponential in voltage differences at its terminals, analogous to reaction rates being exponential in the free energy differences in a chemical reaction; increases in gate voltage lower energy barriers in a transistor increasing current flow analogous to the

TABLE I
SIMILARITIES BETWEEN CHEMISTRY AND ELECTRONICS

Chemical Reaction Dynamics	Electron Flow in Transistor
Reactant Concentration	Electron concentration at the source
Product Concentration	Electron concentration at the drain
Forward and reverse reaction rates in chemical reaction	Forward and reverse current flows in the transistor
Reaction rates are exponential in free energy differences in chemical reactions	Forward and reverse currents in transistor are exponential in voltage differences at its terminals
Enzymes or catalysts in chemical reactions increase reaction rates	Increases in gate voltage lower energy barriers in a transistor, increasing current flow
Stochastics of molecular Poisson processes in chemical reactions [3], [4]	Stochastics of electronic Poisson processes in subthreshold transistors [3], [4]
Flux Balance Analysis	Kirchhoff's Current Law
Chemical Energy Conservation	Kirchhoff's Voltage Law
Chemical Concentration	Current
Electrochemical Potential: Log(Concentration)+Energy	**Electrochemical Potential: Log(Current) + Voltage**

effects of enzymes or catalysts in chemical reactions that increase reaction rates; and, the stochastics of Poisson shot noise in subthreshold transistors are analogous to the stochastics of molecular shot noise in reactions. Table I itemizes several of these similarities.

The logarithmic dependence of the electrochemical potential in chemical concentration or on current enables one to map log-domain analog transistor circuit motifs in subthreshold electronics to log-domain analog molecular circuit motifs in cells and vice versa. If we examine the classic Michaelis-Menten enzyme-substrate binding basis function, we find that

$$\frac{(x/K_d)}{1+(x/K_d)} = \frac{1}{1+e^{-\ln(x/K_d)}}. \tag{1}$$

Therefore, if we look at the left hand side, the basis function may be viewed as being approximately linear and proportional to (x/K_d) for $x < K_d$ and saturating after $x = 10K_d$; or, if we look at the right hand side, it may be viewed as being log-linear over the range $0.1K_d < x < 10K_d$ where the sigmoid is linear. Hence this basis function has a log-linear analog regime of operation over the central portion of the sigmoid and a saturating digital regime at the extremes of the sigmoid (see also Fig. 2). The term $\ln(K_d)$ is proportional to the free energy of the binding reaction. Highly compact eight-transistor log-domain analog differential-pair circuits [3], [27] generate almost exactly identical mathematical basis functions in either the linear current [27] (left hand side of (1)) or log-linear voltage domain [27] (right hand side of (1)). Log-domain analog circuits can generate any polynomially linear or polynomially nonlinear dynamical system in both electronics and in chemistry [3]. In particular, they can generate dynamical systems of the form

$$\begin{aligned} \frac{d\mathbf{x}}{dt} &= \boldsymbol{C} + \boldsymbol{D}\mathbf{x} + \boldsymbol{E}(\mathbf{x}\otimes\mathbf{x}) + \boldsymbol{F}\mathbf{u} + \boldsymbol{G}(\mathbf{x}\otimes\mathbf{u}) \\ \mathbf{y} &= \boldsymbol{H}\mathbf{x} + \boldsymbol{K}\mathbf{u} \end{aligned} \tag{2}$$

where $\mathbf{x}$ and $\mathbf{u}$ are molecular vector state and molecular input variables respectively, the matrix coefficients are determined by chemical-reaction kinetic parameters, and the multiply operations refer to outer products derived from two-molecule chemical binding. The limitation to two-molecule binding is for practicality: Two molecules can bind to generate a complex, and the complex can then bind to a third as is true in most chemical reactions. Generalizations to other reaction types such as dissociation, transformation, substitution or production are included in (2) as well. Although noise is not explicitly represented in (2), the fluxes on the right hand side of (2) are all Poisson in both subthreshold electronic circuits and in chemical reaction networks. Therefore, log-domain 'cytomorphic' circuits can represent the deep connections between electronics and chemistry shown intuitively in Fig. 2 and (1), or mathematically in (2). They can be built to quantitatively model fundamental stochastic protein and DNA circuits in a precise fashion with just a few transistors [3], [27]–[29]. Such analog circuits have already helped port log-domain linearization circuit motifs in electronics [72] to log-domain linearization circuit motifs in cells to build a 'bio-molecular slide rule' or log-domain analog calculator [7]. In the future, such circuits may also help us design robust biological circuits by exploiting feedback techniques from the mature discipline of subthreshold or log-domain analog circuit design [3].

Most readers in the field of synthetic biology today are unfamiliar with transistor circuit design. Therefore, in this review paper, we will focus on using analog circuit schematics that do not use transistors to describe synthetic biological circuits. As we discuss, such schematics may be generated directly from the underlying molecular differential equations (e.g., Fig. 3) and may also be ported to exact cytomorphic circuit equivalents [3] but it is not necessary to do so. A companion paper in this volume describes how cytomorphic transistor equivalents represent molecular basis-function circuits exactly [76]. However, we shall frequently point out similarities between feedback-loop and other motifs in well-known electronic circuits and those in molecular circuits. These similarities will allow us to port robustness, efficiency, dynamics, stochastics, resource-consumption and other circuit insights from electronics to biology in a physical and intuitive fashion without requiring a knowledge of transistor-based electronic design. Readers interested in learning more about feedback systems may find the tutorial in Chapter 2 of [3] useful.

This paper is organized as follows. In Section II, we discuss fundamental examples that represent enzyme-substrate or molecular binding and the basic processes of transcription and translation via analog circuit schematics (Figs. 3 and 4). **We then show how to create a canonical analog circuit schematic that pictorially represents fundamental molecular differential equations at the DNA, RNA, protein, and small-molecule levels** (Fig. 5). Using this canonical analog circuit schematic as a basis, we review 17 circuits in synthetic biology by drawing their analog circuit equivalents in Section III. These circuits typically utilize only portions of the canonical analog circuit schematic (Fig. 5) to operate. They also often only utilize the saturating portions of their basis functions to operate and are thus 'digital' by design, even though the published input-output

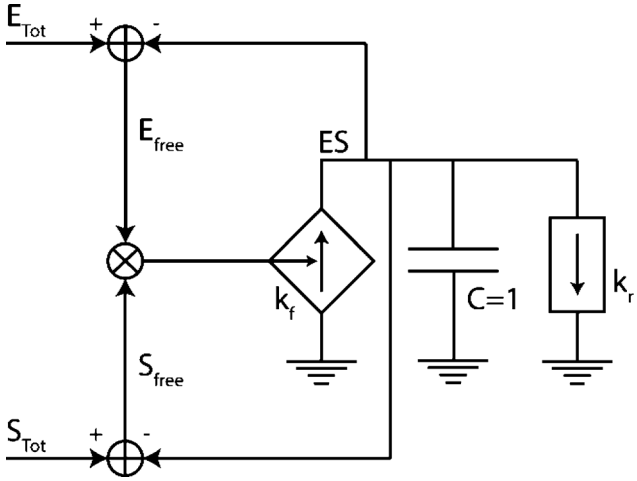

Fig. 3. Enzyme-Substrate or Molecular Binding Circuit. A voltage multiplier takes the amount of free enzyme ($\mathrm{E_{free}}$) and substrate ($\mathrm{S_{free}}$) as inputs and produces a forward Poisson current flux to represent complex (ES) formation. For each ES formed, an equivalent amount of E and S is consumed. This consumption is accounted for by the voltage subtractor, which generates the unbound species as the difference between the total and bound species. The 'use-it-and-lose-it' negative-feedback loops of the subtractor quantitatively account for saturation in enzyme-substrate binding, loading, and resource consumption effects on E_{Tot} and S_{Tot}. A second current generator, a linear conductance proportional to k_r in this case, produces a backward Poisson current flux to represent ES dissociation. Over time, the system reaches a steady state that is determined by equilibrium between the two current fluxes.

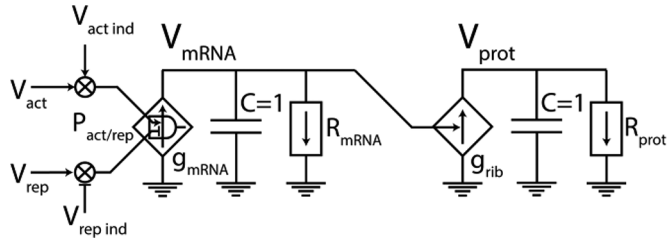

Fig. 4. Elementary Genetic Promoter. The transcription of mRNA, whose concentration is represented by $\mathrm{V_{mRNA}}$, is regulated by transcriptional activators and repressors ($\mathrm{V_{act}}$ and $\mathrm{V_{rep}}$) and the translation of mRNA produces encoded output protein, $\mathrm{V_{prot}}$. The dependent current generators, g_{mRNA} and g_{rib} control production rates of mRNA and protein respectively and the linear or nonlinear resistors, R_{mRNA} and R_{prot}, control degradation of mRNA and protein respectively. In this example, an 'AND' promoter $\mathrm{P_{act/rep}}$ has $\mathrm{g_{mRNA}}$ controlled by two transcription factors, one of which upregulates or increases it and another of which represses or decreases it.

experimental curves invariably illustrate their true analog nature. In Section IV, we review resource consumption in synthetic biological circuits and discuss why analog circuits in nature are efficient in their use of resources. In Section V, we conclude by summarizing the paper.

II. Analog Circuit Representations of Fundamental Bio-Molecular Circuits

Enzyme-substrate binding, or more generally the binding of two molecules to one another, provide an important analog basis function for many biochemical interactions in a cell including the binding of enzymes to metabolites to aid in anabolism (synthesis) or catabolism (degradation); the binding of promoters to DNA during transcription; the binding of ribosomes to mRNA transcripts during translation; the binding of an inducer to receptor proteins or to transcription factors in cell signaling; the binding of proteases and RNAases to proteins and RNA for degradation; and, the binding of monomers to each other in cell regulation. When an enzyme (E) and substrate (S) bind, they form a complex (ES) that raises the concentration of ES while depleting the level of E and S. The molecular differential equation that describes such binding is given by

$$\begin{aligned}\frac{d[ES]}{dt} &= k_f[E][S] - k_r[ES] \\ &= k_f([E_{\mathrm{Tot}}] - [ES])([S_{\mathrm{Tot}}] - [ES]) - k_r[ES].\end{aligned} \tag{3}$$

Fig. 3 shows an analog circuit schematic that exactly represents this differential equation including analog behavior, loading, dynamics, molecular and energy resource consumption, and stochastics. Voltages on the nodes represent the concentrations of molecular species. A multiplier takes the concentrations of free E and S as voltage inputs and controls the production of a forward Poisson current flux proportional to k_f. In the schematic, the difference between total and bound species is obtained using a feedback voltage subtractor, which automatically accounts for resource consumption of E and S, the retroactive loading caused by ES generation on upstream circuits that may determine or generate E_{TOT} and S_{TOT}, and the saturation of multipliers in biochemical binding. The backward Poisson current flux that causes ES to dissociate is represented by a dependent current generator proportional to k_r, a linear 'degradation resistance' in the equation above. In general, in more complex schematics, **the negative-feedback loading loops caused by the 'use-it-and-lose-it' subtractors of** Fig. 3 will not always be shown to avoid cluttering the schematic; but, it should be remembered that such subtractive loops always exist from the outputs of a multiplier to each of its inputs. If the output of ES is itself used in a downstream circuit, an additional dependent current generator attached to C will increase its effective rate of degradation while simultaneously affecting a production rate in the downstream circuit, leading to non-modularity. The value of C, set to 1 in Fig. 3, represents the volume of the compartment in which the molecules are housed. Thus, the same molecular production or degradation rates in a larger compartment lead to smaller concentrations. A stochastic electronic circuit noise analysis of the two white-noise Poisson fluxes per unit bandwidth integrated over the bandwidth of the circuit $(k_f[S_{\mathrm{free}}] + k_r)/C$ (determined by simple feedback root-locus circuit techniques or resistive-divider techniques in [3]) yield the total molecular concentration noise in ES with the charge on the electron, q, being '1'. For the typical case where S is much larger than E, the analysis is described in [3]

$$\begin{aligned}k_f^{'} &= k_f[S] \\ \overline{v_n^2} &= 2qE_t\left(\left(1 - \frac{k_f^{'}}{k_f^{'} + k_r}\right)k_f^{'} + \left(\frac{k_f^{'}}{k_f^{'} + k_r}\right)k_r\right) \\ &\quad \times \frac{1}{(k_f^{'} + k_r)^2} \times \frac{k_f^{'} + k_r}{2\pi C} \times \frac{\pi}{2}\end{aligned}$$

$$\overline{v_n^2} = 4qE_t\left(\frac{k_f' k_r}{k_f' + k_r}\right)\frac{1}{k_f' + k_r} \times \frac{1}{4C}$$
$$= \frac{E_t}{C}\frac{k_f' k_r}{(k_f' + k_r)^2}$$
$$\boxed{\overline{v_n^2} = \frac{E_t}{C}\left(\frac{k_f'}{k_f' + k_r}\right)\left(\frac{k_r}{k_f' + k_r}\right)}. \quad (4)$$

In fact, the total molecular copy-number noise over the entire volume is given by

$$\sqrt{\sigma_N^2} = \left(\sqrt{\frac{E_t}{C}\left(\frac{k_f'}{k_f' + k_r}\right)\left(\frac{k_r}{k_f' + k_r}\right)}\right)C$$
$$\sigma_N = \left(\sqrt{E_t C\left(\frac{k_f'}{k_f' + k_r}\right)\left(\frac{k_r}{k_f' + k_r}\right)}\right)$$
$$\boxed{\sigma_N = \sqrt{N_t p(1-p)}} \quad (5)$$

where $N_t = E_t C$ is the total number of enzyme molecules within the volume compartment C of the reaction, whether bound or unbound, and p is the probability that an enzyme molecule is bound. Thus, we find that the noise is maximized when the probability of an enzyme molecule being bound is 1/2 and minimized when it is near 1 or 0. Intuitively, a chemical reaction that has a forward flux greatly in excess of the reverse flux ($p = 1$) or vice versa ($p = 0$) will exhibit little noise since almost all molecules will be bound or unbound respectively. Similarly, a transport channel in a cell membrane exhibits the least noise when the probability for its opening is near 1 or 0 [5]. For very-low-copy-number circuits, cytomorphic transistor circuits with artificially amplified thermal Poisson noise can replicate molecular circuit behavior faithfully and rapidly [3], [76].

The effect of the total molecular copy number of the various molecules on cellular machinery or on energy consumption is accounted for via resource-precision equations described in Section IV, which are universal in electronics, neurobiology, and cell biology [3], [4], [77]. Typically, genetic promoter circuits that produce molecules such as E_{TOT}, S_{TOT}, as well as protease circuits that degrade them are also involved. As we show in an example in Fig. 10, protease coupling between circuits is accounted for via similar use-it-and-lose-it subtractors as in Fig. 3, w.r.t. a total protease resource.

Fig. 4 shows an analog circuit schematic for an elementary genetic promoter circuit, which describes the stochastic differential equations of production and degradation that correspond to transcription and translation. Dependent current generators model the Poisson fluxes corresponding to production and degradation of mRNA and protein in an analogous fashion to similar generators in Fig. 3. The noise of this analog circuit schematic [3], [4], [29] has been shown to be identical to that of experimentally measured noise in cells [19]. The noise has scaling properties that are similar to that in bipolar transistors [3], [4], [29] with the 'burst factor' in molecular circuits corresponding to the current gain in bipolar transistors. Eight-transistor cytomorphic equivalents of Fig. 4 that replicate experimental data in *E. coli* are described in [27].

Fig. 4 shows that the V_{mRNA} and V_{prot} in analog circuits are analogous to corresponding molecular concentrations. The production of mRNA in this case is controlled by an 'analogic' dependent current generator with two transcription-factor inputs. In this case, the 'AND' in the schematic indicates that the transcription rate is a multiplicative function of each transcription factor's binding probability to DNA. When the input transcription factor concentrations are at saturated values, these probabilities reach 1. The particular example of Fig. 4 shows a repressor input and an activator input that down or up regulate transcription respectively, with each input itself being multiplicatively regulated by an inducer. In the repressory transcription factor shown in Fig. 4, this input is derepressing.

In cases where the mRNA dynamics is fast compared with protein dynamics, it is possible to approximate Fig. 4 with a single dependent current generator that only represents protein dynamics. In such cases, the gain and noise due to mRNA transcription can be incorporated into the gain and noise of this effective protein generator. In other cases, we can still represent the promoter circuit with one input-output protein generator that has more complex internal dynamics due to mRNA; such dynamics is just not explicitly shown but is still accurately represented by the schematic. The current generators can incorporate delays due to the transcription and translation as well.

The use of hierarchical symbolic schematics has enabled analog electronic-circuit designers to effectively manage the complexity of reams of differential equations with pictures that effectively represent quantitatively accurate behavior to any desired level of abstraction. Similarly, 'effective logic gate' representations, e.g., for an XOR built out of internal underlying 'AND' and 'OR' gates are frequently used in digital design.

The multiplicative blocks in Fig. 4 operate in a similar fashion to those in Fig. 3 since they both represent basis functions corresponding to molecular binding. However, the use-it-and-lose-it negative-feedback loops shown explicitly in Fig. 3 (for S_{TOT} and E_{TOT}) are not shown explicitly in Fig. 4 but are understood to be always present whenever molecules bind. Similarly, the degradation and dynamics explicitly shown in Fig. 3 have been neglected in the multipliers of Fig. 4 since they are usually much faster than transcription and translation dynamics. They can be included in more complex schematics if needed.

The power of circuit representations lies in their ability to simultaneously and pictorially represent several interacting effects precisely with very few parameters in a physically and mathematically deep fashion. For example, the dependent current generator in Fig. 4 that represents mRNA or protein production simultaneously determines i) Poisson noise via the value of this current flux; ii) return-ratio robustness via the derivative of this current flux with respect to its control parameter and by the action of this current flux on the rest of the circuit [3]; iii) ATP and polymerase consumption rates, that are directly proportional to this flux [4]; and iv) loading of this circuit on its previous circuit via the value of the number of control

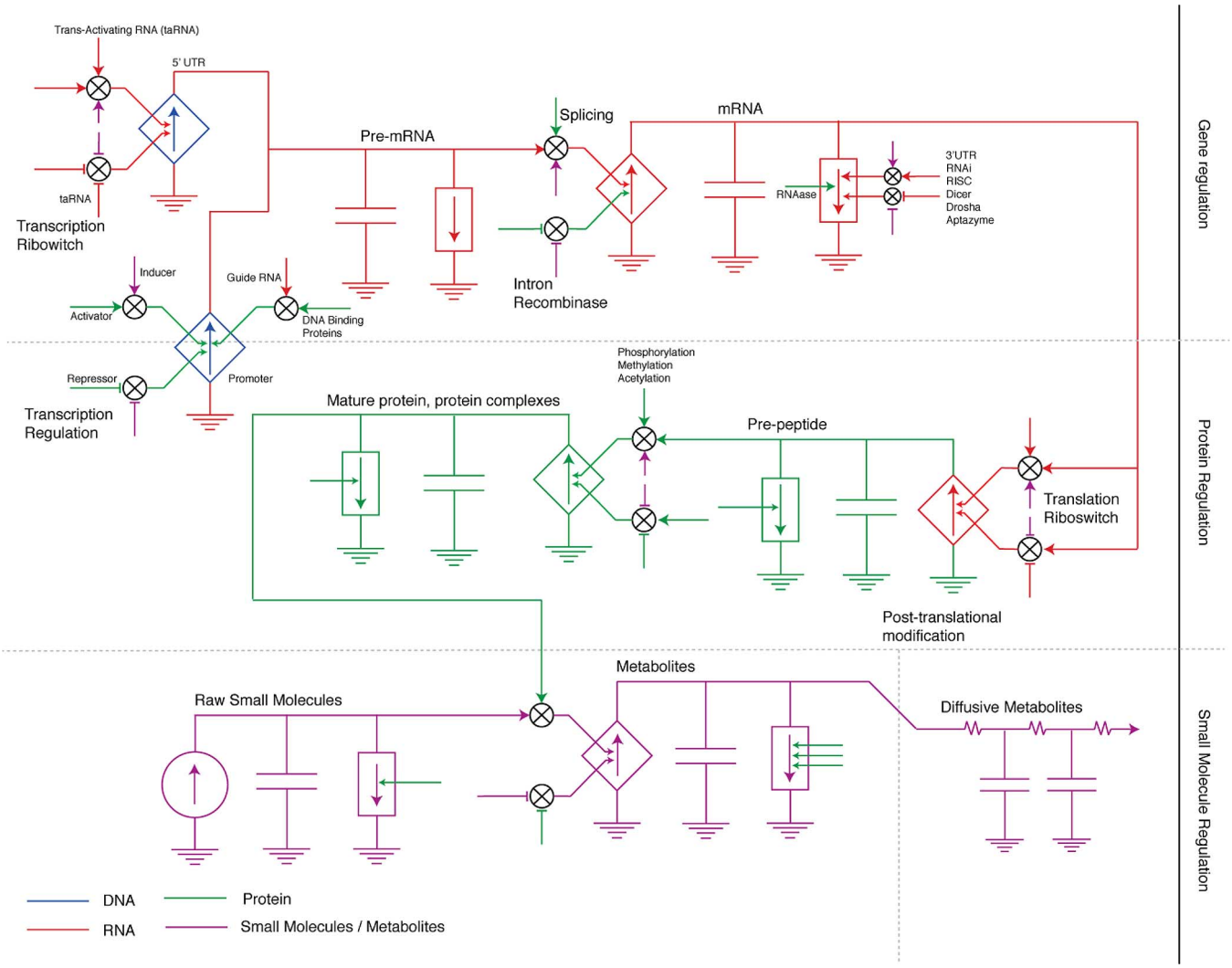

Fig. 5. A Canonical Analog Circuit Schematic for Synthetic and Systems Biology. The schematic represents circuits that have been published at the DNA (blue), RNA (red), protein (green), and small-molecule (purple) levels. It includes circuits such as ribosome switches via taRNA, crRNA, interactions involving RNA degradation via 'ribozymes', splicing control circuits, translational and transcription-based riboswitches, transcription factors built with RNA and guide proteins like CRISPR, metabolites processed by protein enzymes etc.

molecules that are bound to the DNA promoter compared with the total number of control molecules.

Physically correct representations with very few parameters are important in ensuring that the model does not over-fit data while still capturing important dynamics so that the model retains high descriptive and predictive power without losing generality. For example, a physical model of the vocal tract [30] can represent many effects with very few parameters that a Hidden Markov Model takes significantly more parameters and resources to do. Therefore, vocal-tract-based analysis-by-synthesis recognition of speech generalizes better in noise and is more robust and efficient than Hidden Markov models [31].

Using the analog circuit motifs developed above, we have created a canonical circuit schematic to succinctly capture a wide range of molecular circuits, whether at the DNA, RNA, protein, or small-molecule level. Fig. 5 **shows a general schematic representation of circuits at the DNA (blue), RNA (red), protein (green), and small-molecule (purple) level**. We shall use this color convention throughout the rest of this paper when we review other circuits. This circuit schematic is based on the universal basis functions of molecular binding [3]. It was created by examining a large number of published circuits that were fundamentally different in the synthetic biology or systems-biology literature, e.g., ribosome switches via taRNA, crRNA, interactions involving RNA degradation via 'ribozymes', splicing control circuits, translational and transcription-based riboswitches, transcription factors built with RNA and guide proteins like CRISPR, metabolites processed by protein enzymes etc. From schematics such as those in Figs. 3, 4, 5, and others, one realizes that analog circuits can compose any biochemical network in a scalable fashion. They can represent complex stochastic, feedback, nonlinear, loading, and resource-consumption effects independent of the molecular level that the circuit operates at. The molecular level merely serves as a 'label' that determines typical concentration ranges, copy numbers, time constants, gain and other parameters but does not fundamentally alter the structure of the basis functions or the core underlying differential-equation mathematics of

biochemistry. Therefore, Fig. 5 shows that common circuit topologies recur at the blue, red, green, and purple levels. At the purple level, the distributed-RC circuit rigorously represents the partial differential equations of diffusion as is well known in circuit theory [3]. Diffusion has been used for communicating between cells, e.g., in Fig. 10. In the past, distributed circuit models on working silicon chips have even quantitatively modeled sophisticated traveling-wave partial differential equations that describe inner-ear active fluid mechanics [79], which are significantly more complex than simple diffusion. In *in-vitro* or cell-free synthetic biology [92], sometimes DNA itself may be degraded. Such degradation can be captured by adding 'blue degradation elements' to the schematic in Fig. 5.

III. Review of Circuits in Synthetic Biology

In the following discussion, we will review some of the essential circuits that have helped shape the field of synthetic biology with analog circuit schematics. The use of these schematics can shed physical insight into the operation of these circuits; establish connections between artificial and natural circuits that predict new phenomena in biology from old electronic knowledge; and also provide a unifying perspective w.r.t. underlying common themes and motifs in topologies that may appear different. Using the canonical circuit schematic of Fig. 5, we shall begin by focusing on circuits where the control is primarily at the 'blue DNA level', then at the 'red RNA level', and finally at the 'green protein level'. Some of the circuits operate at multiple levels and most use purple inducer inputs.

A. DNA-Based Circuits

Early circuits in synthetic biology and most circuits today use well-characterized DNA-based transcriptional regulation to function. Such circuits consist of multiple DNA promoters that interact with one another via their regulating input proteins and encoded output proteins: Each promoter's encoded output mRNA transcript production and thus translated output-protein production is regulated by input transcription-factor proteins that bind to it. Activator transcription factors up-regulate encoded protein production while repressor transcription factors down-regulate encoded protein production respectively. Small-molecule inducer inputs in turn control the activity or effectiveness of the activators and repressors and thus their ability to regulate transcription. The small-molecule inducer inputs typically enable access to the internal regulatory workings of the cell from its outside. Circuits and feedback loops of interacting promoters (or proteins) are created because the encoded output protein of one promoter can serve as the regulatory input protein of another promoter thus wiring molecules together into networks. For example, in the special case where the encoded output protein and input regulatory protein are one and the same, an auto-regulatory feedback loop can be created. We now review several examples of such circuits.

1) The Latch or Toggle Switch: The toggle switch [32] is one of the earliest circuits in synthetic biology. It functions by configuring two different repressor-encoding promoters, e.g., with encoded proteins LacI and TetR, such that each represses transcription from the other as shown in Fig. 6. The resulting cross-inhibitory positive-feedback loop then leads to bi-stability

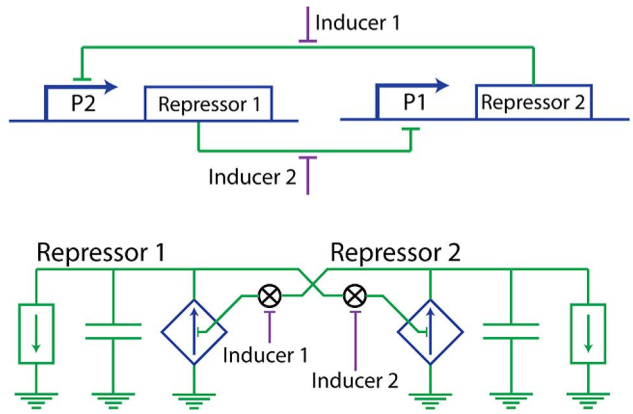

Fig. 6. The Latch or Toggle Switch [32]. This circuit uses a cross-inhibitory positive-feedback loop to produce switch-like behavior. To design the positive feedback loop with bi-stability, two different repressors were configured to cross-inhibit each other; when repressor 1 expression level is high, it represses the expression of repressor 2, which further increases repressor 1, and vice versa. The states can be switched by using inducers that derepress their respective targets.

and preserves digital state as in a classic SR digital latch in electronics: One promoter at relatively high protein-production level represses the other promoter at a state of relatively low protein-production level thus weakening the weak production and strengthening the strong production even more; the resulting win-lose battle favors the initially high repressor and ends in a 'high-low' repressor configuration via positive feedback. The 'high-low' state may be switched by a transient input inducer pulse that binds to and reduces the activity of the high repressor; when this activity is reduced sufficiently, the low repressor recovers in level sufficiently until it is strong enough to shut off the formerly high repressor, which is now at a disadvantage due to its inducer being present. Once the switching has occurred, the transient inducer pulse may be removed and the circuit will remember its digital state. The IPTG small-molecule inducer functions to weaken the activity of the LacI transcription factor, and thus helps TetR to go high, while the aTc small-molecule inducer functions to weaken the TetR transcription factor, and thus helps LacI to go high.

It is worth noting that the high repressor must be constantly produced and degraded, unlike in a classic CMOS SR latch where it costs little energy to maintain state, only to switch it. In that sense, this circuit functions more like an NMOS or PMOS latch with resistive load. More exactly, the nonlinear behavior of the circuit schematic of Fig. 6 is well represented by cross-inhibitory differential-pair circuits configured in a positive-feedback loop with tail currents representing the saturating rates of production of the repressors. Such cytomorphic differential-pair-like circuits fit experimental data for the LacI repressor in *E. coli* well including the ability to mimic Hill coefficients seen in the biological data [27]. The metastable state for switching occurs when the pair of repressor levels is near $(K_{dLacI}([\mathrm{IPTG}]), K_{dTetR}([\mathrm{aTc}]))$ where K_{dLacI} and K_{dTetR} are *effective* inducer-dependent DNA-binding constants of the respective transcription factors. As in electronic circuits, the positive-feedback loop gain [3] must be greater than 1 at this point for bi-stability to occur.

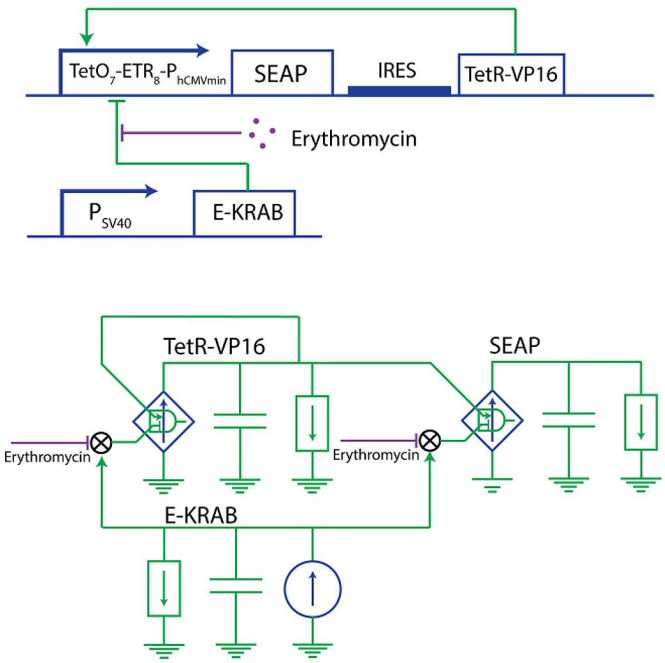

Fig. 7. An Auto-regulating Positive-Feedback Circuit [35]. TetR-VP16 trans-activator (tTA) binds to its hybrid promoter $\mathrm{TetO_7\text{-}ETR_8\text{-}P_{hCMVmin}}$ and induces the expression of human placental secreted alkaline phosphatase (SEAP) and tTA. The expression is repressed by a constitutively expressed fusion protein, E-KRAB, which is inhibited by erythromycin. At low concentrations of erythromycin, SEAP expression level is strongly repressed. Once erythromycin concentration passes a threshold, it induces SEAP expression, which is kept high by tTA's positive auto-regulatory loop. To return to a state of low SEAP expression, the erythromycin level needs to drop below a lower threshold to account for the persistence of the positive feedback. Hence the circuit produces hysteretic behavior w.r.t. erythromycin switching thresholds.

2) An Auto-Regulating Positive-Feedback Circuit: Fig. 7 shows an auto-regulating positive-feedback circuit [35]. The core of this circuit is a transcription factor TetR-VP16 that auto activates its own transcription. The molecule SEAP (Secreted Alkaline Phosphatase) serves as both a reporter molecule, i.e., a molecule with a concentration that is a monotonically increasing function of TetR-VP16, as well as an effector enzyme molecule, in this case as a phosphatase enzyme that dephosphorylates its substrate. As in the latch, this circuit will exhibit instability if its positive-feedback loop gain is greater than 1, which can only occur if the levels of TetR-VP16 are sufficiently high. Switching of state in this circuit is enabled by a repressing transcription factor, E-KRAB that acts with TetR-VP16 at the 'AND promoter' to reduce transcription and lower the loop gain of the positive-feedback loop. At relatively high levels of the repressor, levels of TetR-VP16 are attenuated as the positive-feedback loop is weakened. The constitutive or unregulated production of E-KRAB is represented by the circular (non dependent) current source in Fig. 7. Like the IPTG-LacI inducer-repressor pair in the previous section, the activity of the E-KRAB repressor is modulated by the small-molecule inducer erythromycin, a macrolide antibiotic, which like IPTG, also has a derepressing effect.

A system is said to exhibit hysteresis if it possesses state-dependent thresholds for switching from one state to another. Positive-feedback loops exhibit hysteresis because parameters of the circuit are altered by its existent state such that conditions for switching one state to another are different in different states. Examples in biology include positive-feedback loops in cell-cycle transitions [33] that manifest hysteresis. As in the positive-feedback loops in electronics that ensure that small levels of noise do not cause jittering and oscillation between states when parameters or inputs are right near the switching-threshold levels, such hysteresis ensures robust unidirectional state transitions in cells. Similarly, positive-feedback loops in evolutionary dynamics manifest hysteresis such that the environmental conditions that lead to population collapse are different from the environmental conditions necessary for recovery [34].

The circuit of Fig. 7 exhibits hysteresis as well: When the erythromycin concentration is low, the E-KRAB repressor is effective at maintaining TetR-VP16 at a low level. When the erythromycin concentration increases past a threshold, derepressing and thus reducing the activity and effect of E-KRAB, the TetR-VP16 auto-activating positive-feedback loop goes unstable and eventually saturates at a high level of TetR-VP16 (and SEAP) expression. To now switch the circuit back to its low level of expression, the high-to-low switching threshold of erythromycin is lower than the low-to-high switching threshold of erythromycin: Formerly, the repression of E-KRAB just needed to be weakened enough to enable the leaky basal expression level of TetR-VP16 to auto-activate the positive-feedback loop. Now, the repression of E-KRAB has to be strong enough to enable the high expression level of TetR-VP16 to fail to activate the positive-feedback loop.

This example illustrates why positive-feedback loops are usually built like an SR latch in electronics and rarely via an auto-activating transcription factor as in this example: If the leaky expression level of the TetR-VP16 is not high enough, the loop may never activate and permanently remain at low levels of expression, necessitating a separate 'startup circuit' for circuit operation to be robust. In contrast, precisely because on/off ratios are never that high in biology, Fig. 7 does not need an explicit startup circuit. The need for leaky expression does suggest that this circuit may not always be robust in other contexts.

3) The Repressilator or Ring Oscillator: Oscillation is a recurring biological phenomenon that is associated with many cellular processes. Examples include encoding information in the calcium signaling pathway [36], keeping time in circadian clocks [37], and forming spatial patterns in organisms [38]. Early pioneering work in synthetic biology created an oscillatory network using three transcriptional repressors LacI, TetR and cI in a negative-feedback loop as shown in Fig. 8 [39]. The circuit is widely known as the 'Repressilator'.

As in ring oscillators in electronics, formed with an odd number of inverting stages in a loop, the Repressilator requires an odd number of repressory stages for generating oscillations. As standard feedback root-locus theory for circuits predicts [3], oscillations are favored by high-loop-gain conditions including strong promoters and closely spaced degradation time constants in the loop including those for mRNA and proteins. Just as in electronic feedback circuits, the presence of mRNA and protein delays in the loop can reduce the critical loop gain needed for an oscillation. Each of the three inverting stages has different input K_d and output levels. The three inducers, namely IPTG,

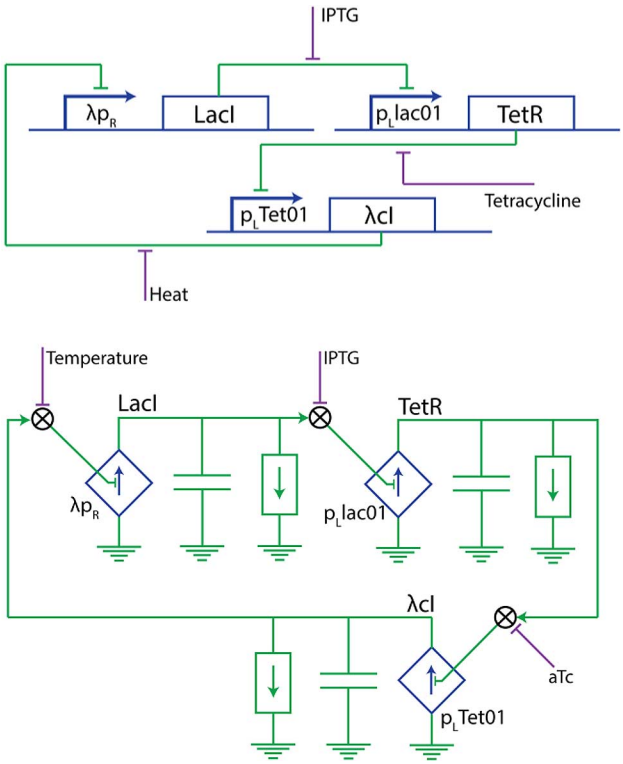

Fig. 8. The Repressilator or Ring Oscillator [39]. This three-repressor circuit is comprised of LacI, TetR and cI. Their target promoters are $p_L$lac01, p_LTet01 and λcI respectively. TetR represses cI expression, cI represses LacI expression, and finally LacI represses TetR expression, thus completing the negative-feedback loop. Depending on the loop gain and loop delay, the repressilator may oscillate or decay to a steady state.

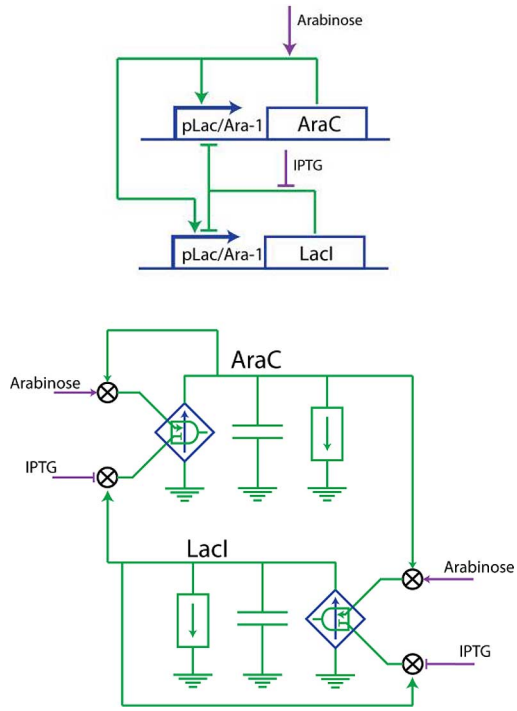

Fig. 9. A Tunable Relaxation Oscillator [40]. The circuit is comprised of activator AraC, repressor LacI and a hybrid promoter pLac/Ara-1 that is regulated by and drives the transcription of both genes. The presence of an auto-regulatory positive feedback loop on AraC, and a negative-feedback loop between LacI and AraC gives rise to oscillatory behavior. Both AraC and LacI respond to inducers arabinose and IPTG respectively, which can be used to tune the periodicity of the oscillations.

aTc, and temperature, which modulate transcription-factor activity, can help to ensure that the output of one stage is at a level that enables its following stage to operate with sufficient gain. A more accurate analogy to this circuit is a cascade of three current-mode differential-pair circuits like those described in [3], [27].

A repressilator's oscillation period is primarily governed by the sum of the delays of the inverting stages in its feedback loop, which in turn are primarily governed by the effective inducer-dependent DNA-binding K_d's, transcription and translation delays, and degradation time constants of each of its gain stages. Hence, as in electronics, such oscillators are not as easily tunable as oscillators built with other topologies whose oscillation period does not depend on a complex combination of multiple parameters.

4) A Tunable Relaxation Oscillator: Some of the simplest oscillators in electronics are relaxation oscillators: Such oscillators use fast positive feedback to architect transitions between two states and slower negative feedback to determine the duration of existence in each state. Fig. 9 shows a similar molecular relaxation oscillator topology [40]: Here, AraC with an arabinose inducer, auto activates its own production but also causes the production of LacI, which then represses AraC production via a delayed negative-feedback loop. As usual, LacI is derepressed by an IPTG inducer. One unusual feature of the circuit in Fig. 9 compared to traditional relaxation oscillators is that it also has an additional minor negative-feedback loop where LacI represses its own production via auto-repression.

Strong auto repression attenuates the input-output function of the minor negative-feedback loop, which weakens the overall loop gain of the major negative-feedback loop. Thus, as IPTG concentration increases, LacI auto-repression is weakened and the loop gain of the major negative-feedback loop is increased, which is effective in counteracting the positive-feedback loop sooner, such that the oscillatory period falls. In contrast, as arabinose concentration increases, the positive-feedback loop is strengthened, the major negative-feedback loop takes longer to counter the stronger positive feedback, and the oscillatory period rises.

Any minor negative-feedback loop with delay (due to transcription or translation or both) and a loop gain greater than 1 will oscillate; two time constants in a major negative-feedback loop with delay and two gain stages is even more prone to oscillation; and, positive feedback with delayed negative feedback increases major loop gain and causes instability and oscillation via a relaxation-oscillator mechanism [3]. Thus, the circuit of Fig. 9 is quite prone to oscillation via three independent mechanisms that synergize. Consequently, unlike the repressilator that requires relatively careful inducer tuning to ensure that the loop gain in one negative-feedback loop is sufficiently high to trigger oscillation, the oscillations in this circuit persist for a large range of inducer concentrations. Hence, the presence of oscillation is more robust to inducer parameter variations in the circuit of Fig. 9 than in the circuit of Fig. 8.

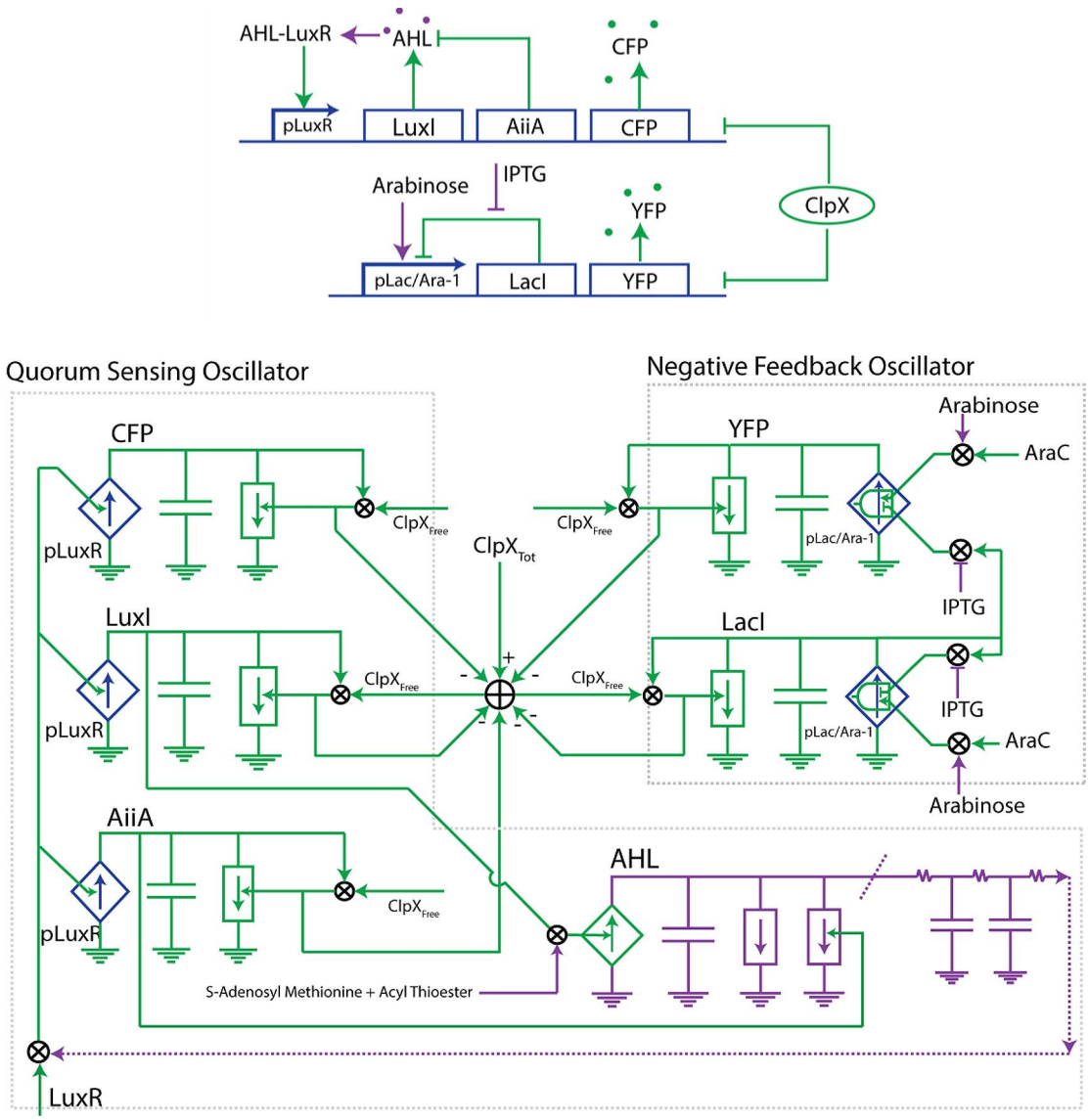

Fig. 10. A Protease-Coupled Collective Oscillator [18]. The circuit couples a negative-feedback oscillator (intracellular) and a collective quorum-sensing oscillator (involving many cells in a colony). *Negative-feedback oscillator*. LacI inhibits its own expression, forming an auto-regulatory negative feedback loop. AraC-arabinose induces LacI expression. If the circuit has a delay and loop gain greater than 1, it will produce oscillations. *Quorum sensing oscillator*. The oscillator expresses LuxI and AiiA, which increase and degrade AHL respectively to form a relaxation oscillator with positive and negative feedback. The AHL-LuxR complex binds to pLuxR and drives the transcription of LuxI and AiiA, simultaneously creating the positive and negative feedback loops. The diffusible molecule AHL synchronizes oscillations amongst cells in the colony and increases collective loop gain in the quorum sensing oscillatory. *Coupling*. All molecules, except LuxR, are tagged with the LAA degradation tag, which causes them to share a common ClpX protease tag and couple via a global use-it-and-lose-it ClpX-based negative-feedback loop.

5) A Protease-Coupled Collective Oscillator: The protease-coupled oscillator of Fig. 10 is an elegant circuit that utilizes transcription-factor, protease, and small-molecule interactions to function [18]. It is comprised of a colony of several cells that exchange a small-molecule AHL inducer (N-Acyl homoserine lactone) amongst themselves to synchronize relaxation oscillators within each of them, increasing their propensity to create more AHL if there is more AHL in the environment and thus increasing the positive-feedback loop gain of each relaxation oscillator. Thus, as in a laser that also has collective positive feedback (amongst resonant atomic oscillators versus relaxation cellular oscillators), there is a critical quorum or colony size or cell-density that excites a collective oscillation: the collective positive-feedback loop gain must exceed 1 for the oscillation to trigger just as there is a critical population-inversion threshold in a laser for an oscillation to excite. This collective 'quorum-sensing oscillator' utilizes both LuxI, which catalyzes the production of AHL and serves to implement positive feedback, and lactonase AiiA, which degrades AHL, and serves to implement the delayed negative feedback characteristic of a relaxation oscillator. AHL is a highly diffusable molecule that is secreted by the cell, which makes it an ideal messenger for cell-cell signaling. LuxI and AiiA genes are both linked to the pLuxR promoter, which is activated by the LuxR-AHL complex as shown in Fig. 10. In addition to this quorum-sensing (QS) oscillator, each cell also contains a negative-feedback (NFB) oscillator, architected by LacI-mediated auto repression and implicit delay. As long as there is delay and a loop gain greater than 1, the

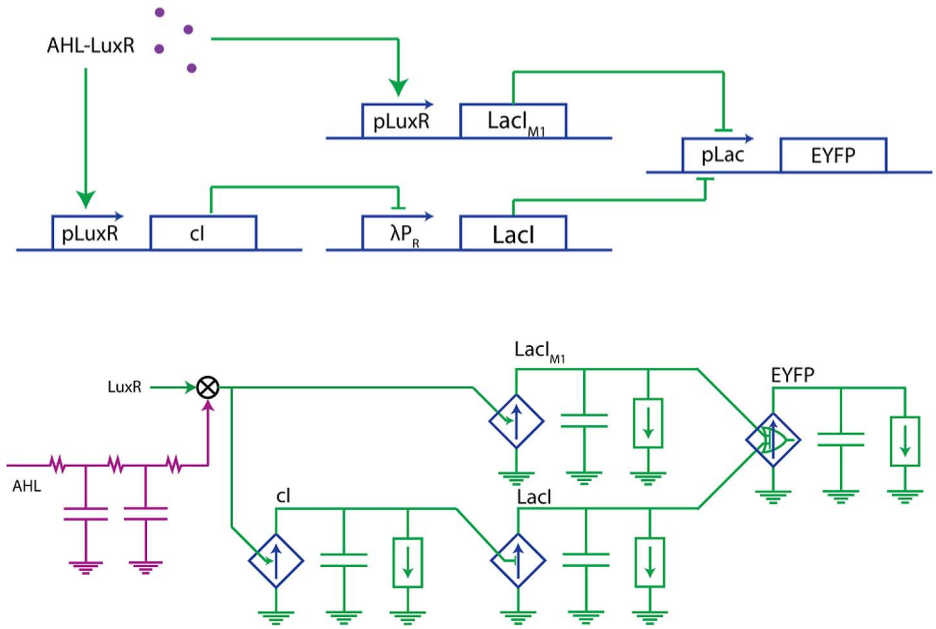

Fig. 11. A Band-Detect Feed-Forward Loop [41]. The circuit uses an incoherent feedforward loop to generate an output that is dependent on the concentration of AHL in the environment. At low concentrations of AHL, the AHL-LuxR complex does not generate enough cI to repress LacI production; thus LacI inhibits EYFP production at the 'OR' EYFP promoter. At high concentrations of AHL, the AHL-LuxR complex induces $\mathrm{LacI_{M1}}$ expression, which inhibits EYFP. EYFP is expressed only at an intermediate level of AHL-LuxR concentration such neither LacI nor $\mathrm{LacI_{M1}}$ is at a concentration strong enough to repress EYFP.

negative-feedback oscillator will excite, but on a significantly faster time scale than the slower collective quorum-sensing oscillation.

One interesting innovative feature in this circuit is an ingenious mechanism for coupling the two oscillators to one another. The mechanism uses protein-degradation resource coupling within the cell, mediated by a common ClpX protease that is shared by all proteins that bind to the protease and are consequently degraded by it. The resulting ClpX use-it-and-lose-it negative-feedback loops then result in the analog circuit schematic of Fig. 10 as in all biochemical binding reactions. Indeed, these loops arise via an identical mechanism to the use-it-and-lose-it negative-feedback loops in the classic biochemical binding circuit of Fig. 3: S_{TOT} and E_{TOT} function as common shared biochemical binding resources in Fig. 3 versus $ClpX_{\mathrm{TOT}}$ in Fig. 10. The coupling occurs at a rapid time scale, significantly faster than the time scale of either oscillation.

The two oscillators serve to couple to one another because the use of the ClpX protease by a high level of LacI in the fast NFB oscillator reduces ClpX binding to the AHL-synthesizing LuxI in the slow QS oscillator, causing lower degradation of LuxI, and thus also making LuxI higher in value. Thus, certain manipulations that increase LacI levels (such as a low level of IPTG that increases NFB loop gain and LacI oscillation amplitude in Fig. 10) lower the frequency of the fast NFB oscillation but help the resulting higher LuxI level trigger the QS oscillation sooner, and consequently increase the QS oscillator frequency. In turn, the high LuxI levels during the slow QS oscillation drive the LacI levels in the NFB oscillator into a high-saturated value that strongly attenuates the strength of its negative-feedback loop and temporarily stops fast NFB oscillation. The overall coupling and synchronization between the oscillators lowers the variability in NFB oscillation significantly. The increase in LuxI levels caused by the NFB oscillator promotes triggering of the QS oscillation more easily making it occur at effectively lower cell densities.

The circuit of Fig. 10 is a fine example of how analog feedback circuits at the blue, green, and purple levels, and at multiple time scales synergize and conspire to create interesting nonlinear dynamical and control systems.

6) A Band-Detect Feed-Forward Loop: Fig. 11 illustrates a feed-forward loop (FFL) [90] that effectively creates a 'band detect' function for a diffusive small-molecule AHL input entering the cell: the circuit output responds to an AHL input only within a certain band of concentration values that is not too low and not too high [41]. AHL entering the cell binds to a transcription-factor LuxR to create an AHL-LuxR complex. The AHL-LuxR complex up-regulates both $\mathrm{LacI_{M1}}$ (a mutated and less sensitive version of LacI) and cI production. The cI down-regulates LacI production. The overall circuit is termed an 'incoherent feed forward loop' since one pathway (via $\mathrm{LacI_{M1}}$) has a sign that will, in the long term, repress EYFP production in response to its LuxR-AHL input, while another pathway (via cI and LacI) has a sign, that will, in the long term, activate EYFP production in response to the same LuxR-AHL input. Other FFLs can be coherent where both pathways have the same sign [90]. Both pathways combine at the 'OR' EYFP promoter, where either the $\mathrm{LacI_{M1}}$ or LacI repressor can repress production of EYFP. The net effect is that, at high AHL, the relatively insensitive $\mathrm{LacI_{M1}}$ pathway will repress EYFP production; at low AHL, the LacI pathway will repress EYFP production because cI has not been produced at a concentration that is strong enough to repress LacI production; at intermediate AHL, neither pathway represses EYFP production. Thus, only intermediate values of AHL input lead to an EYFP output, making this circuit a 'band detector' of AHL input.

This 'digital NOR circuit' was used to architect interesting spatial patterns [41] in a manner analogous to the more analog reaction-diffusion equations first pioneered by Alan Turing [38]: A central source of AHL diffuses radially and, within a certain banded circumferential zone of the center where AHL is not too high or not too low, cells expressing fluorescent EYFP glow. Controlled spatial pattern formation with multiple centers and multiple fluorescent colors were also architected. An interesting experimental observation was that non-equilibrated circuit dynamics could cause bands to move w.r.t. the center and change their locations. The RC dynamics in the analog circuits of Fig. 11 as well as the distributed-RC diffusive dynamics in Fig. 11 can help design and analyze such pattern formation.

Like XOR-based one-shot circuits in electronics that are used to generate pulses, the circuit of Fig. 11 can exhibit 'glitches': For example, a sudden and abrupt decrease in AHL input can reduce $\mathrm{LacI}_{\mathrm{M1}}$ causing EYFP to be expressed; since cI does not fall instantly, and LacI does not build instantly, EYFP will continue to remain high for a while causing a 'transient glitch'. Hence, even in relatively digital circuits, analog circuits are important in analyzing diffusive and circuit dynamics.

7) Log-Linear Analog Computation: The cytomorphic mapping shown in Fig. 2, (1) and (2) enable us to also map Boltzmann log-domain electronic circuit motifs to Boltzmann log-domain biological circuit motifs in a principled fashion in the future. Logarithmic transduction affords advantages such as constant-precision sensing at any intensity (Weber's law) and is seen in many natural systems including audition, vision, and in cells. To widen the dynamic range of input operation of an inducer, it is useful to have a wide log-linear range rather than the two-order-of-magnitude log-linear range typically observed for (1). Versions of (1) with a higher Hill coefficient have even less log-linear range, e.g., just half an order of magnitude for a Hill coefficient of 4.

If the concentration of a transcription factor is fixed, as the inducer increases in value, it will eventually be bound to all the available transcription-factor molecules and saturate the number of bound inducer-transcription-factor complexes that are possible. In addition, if the number of DNA binding sites for a complex are limited, these sites will eventually all be bound by complexes and gene expression will saturate. These two sources of saturation limit the log-linear dynamic range of inducer operation. Fig. 12 shows a genetic circuit motif [7] and an associated analog circuit schematic that simultaneously alleviates both these saturation problems to widen the log-linear dynamic range.

In Fig. 12, a positive-feedback loop increases the generation of transcription factor by catalyzing its own production on a low-copy plasmid. As the amount of inducer increases, more transcription factors are created alleviating saturation of complexes. The high-copy plasmid has several binding sites that also shunt away the complexes, thus alleviating saturation of DNA binding sites on the low-copy plasmid. The high-copy plasmid also serves to control the gain of the positive-feedback loop by altering the number of complexes available to the low-copy plasmid. Such control exploits 'the fanout loading' of the downstream high-copy plasmid on the upstream low-copy plasmid

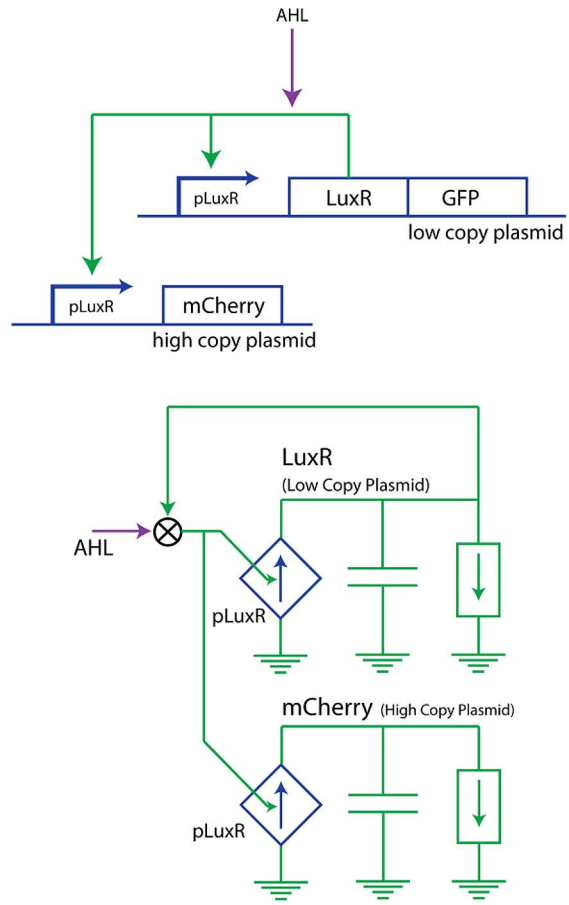

Fig. 12. A Linearizing Analog Circuit Motif [7]. The circuit combines graded analog positive feedback via the low copy plasmid (LCP) and the high-copy decoy plasmid (HCP) to create an expansive nonlinearity that compensates for compressive saturating nonlinearities in inducer-transcription-factor and transcription-factor-DNA binding to create a log-linear input-output function [7]. It is similar to another linearizing analog circuit motif in electronics [72].

as a desirable feature in our analog circuit. Fanout is often a problem in molecular digital circuits.

The genetic circuit of Fig. 12 actually exploits an idea from subthreshold (Fig. 2 corresponds to a subthreshold transistor) log-domain analog circuit design reported in [72]: Expansive $sinh$-based linearization of compressive-and-saturating $tanh$-based differential-pair circuits causes them to widen their linear range of operation [72]. The function of the $sinh$ is achieved by positive feedback in Fig. 12 and the function of the $tanh$ is analogous to that of the saturation of biochemical binding. Indeed, in the future, other linearization circuit motifs from log-domain circuit design, e.g., those in [3] could also be ported to cells. The Supplementary section of [7] models how, analogous to the case in electronics [72], widest dynamic range in the circuit motif of Fig. 12 is achieved at an optimal value of positive feedback.

Fig. 13 and its associated schematic show how to use logarithms to divide by using $\log(\mathrm{A}) - \log(\mathrm{B}) = \log(\mathrm{A}/\mathrm{B})$: Two linearized positive-feedback circuit motifs enable two inducers, Arab and AHL, to effectively control the expression of the mCherry fluorescent protein on the high copy plasmid. The Arab input controls mCherry by *activating* its production. The AHL input generates LacI on the low-copy plasmid, which

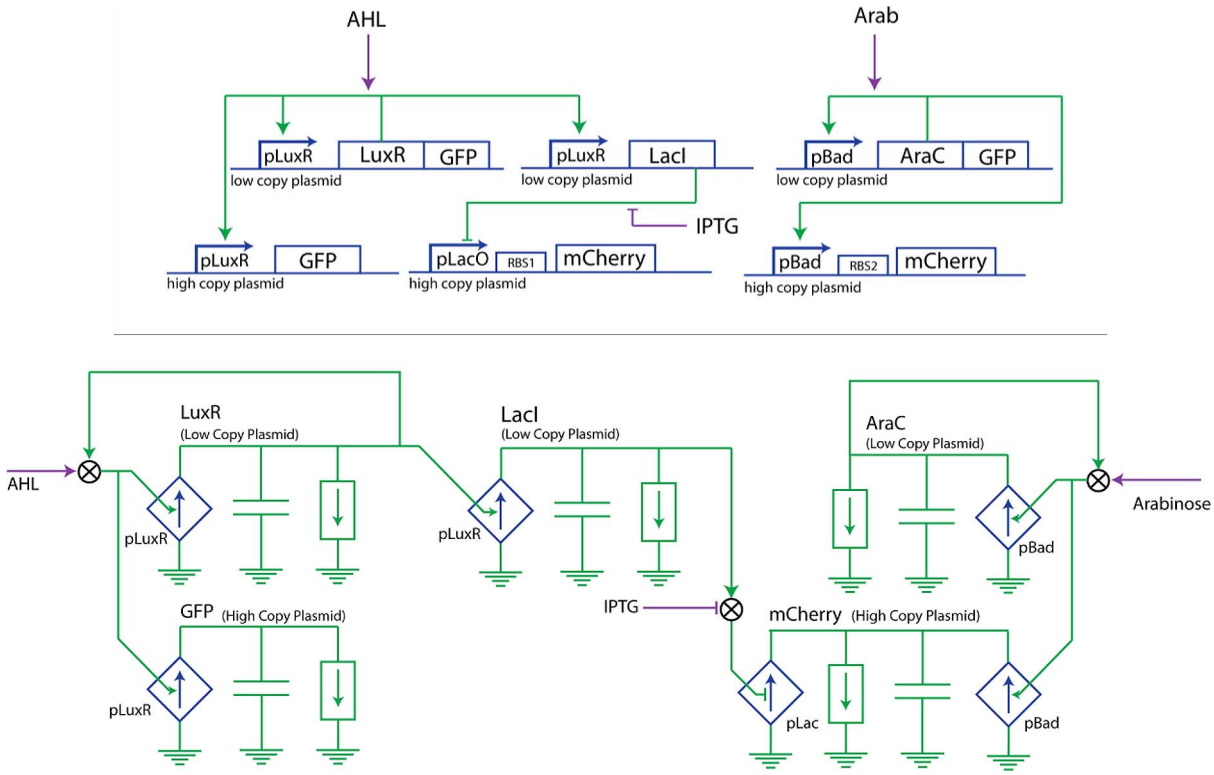

Fig. 13. A 'pRatio' circuit for a 'biomolecular slide rule' [7]. This circuit demonstrates how subtracting logarithmic inputs can effectively encode a division operation as in a slide rule [7]. It combines two different log-linear circuits from Fig. 12, wherein one circuit activates mCherry expression, while the other activates LacI expression, and thus represses mCherry expression. The Ribosomal Binding Sites of mCherry (RBS1, RBS2) help ensure that the slope-magnitudes of each logarithmic contribution are nearly matched.

then *represses* mCherry production. The IPTG inducer fine tunes this repression gain. The RBS1 and RBS2 translation gains (analogous to g_{rib} in Fig. 4) also serve to fine tune the gain of the positive logarithm w.r.t. the gain of the negative logarithm. The net result is that the logarithmic ratio of the two inducer molecules is obtained over almost four orders of magnitude. This 'pRATIO' circuit, generalizes the concept of pH, a logarithmic ratio used to measure $\mathrm{H}+$ concentration w.r.t. a reference, to any arbitrary ratio of two inputs w.r.t. one another. It may have applications for the wide dynamic range sensing of biomolecules by serving as a log differential amplifier.

In log-linear systems, the computational basis functions needed for universality besides the logarithm itself are addition, subtraction, and scaling. The [7] shows how to architect logarithmic addition by merely summing fluxes. Fig. 13 shows to implement logarithmic subtraction. Scaling is also implicit in Fig. 13 (via the IPTG, RBS1, and RBS2 gains). The equivalent of addition, subtraction, and scaling with logarithms corresponds to multiplication, division, and power laws in the linear domain, much as in the operation of slide rules. The [7] discusses how to implement a square root with only two transcription factors, $65\times$ more efficient in part count than a heroic *in-vitro* digital implementation that used 130 parts. It is likely that synthetic biology will benefit from other such efficient analog circuits in the future.

B. RNA-Based Circuits

Transcriptional genetic networks are simple yet versatile, so they have often been the medium of choice when designing synthetic circuits. However, such circuits typically place a significant metabolic strain on the host since each protein regulator undergoes synthesis and degradation constantly [4]. Recently, the use of programmable RNA parts for genetic-engineering has started gaining traction among synthetic biologists. Both DNA and RNA are capable of catalyzing enzymatic reactions, tuning transcription and translation, undergoing self-cleavage, and much more. Nucleic acids are easy to program and synthesize, which make them an attractive target for synthetic biology [42]. We will discuss the mechanisms of a few RNA devices, and how they have been incorporated into synthetic circuits. Since this review focuses primarily on circuits in living cells, we shall not review other excellent work on *in-vitro* synthetic biology that has used DNA and RNA including strand-displacement and catalytic- hairpin-assembly circuits [47]–[51]. Readers may consult the latter references for an excellent introduction.

In living cells, RNA copy numbers are typically quite low, and the on/off ratios of most devices are lower than those of DNA-based devices. Therefore, analog and stochastic computation becomes quite important in RNA-based circuits, even if they are designed to be 'switches'.

One important RNA device that regulates gene expression post-transcriptionally in eukaryotic cells is the microRNA (miRNA). Since it does not code for a protein, miRNA is also called a non-coding RNA (ncRNA; miRNAs are often $\sim$22 nucleotides long and are optimized for both binding affinity and specificity [43]. In eukaryotic cells, miRNA binds to Argonaute, a protein in the RNA-induced silencing complex (RISC), and

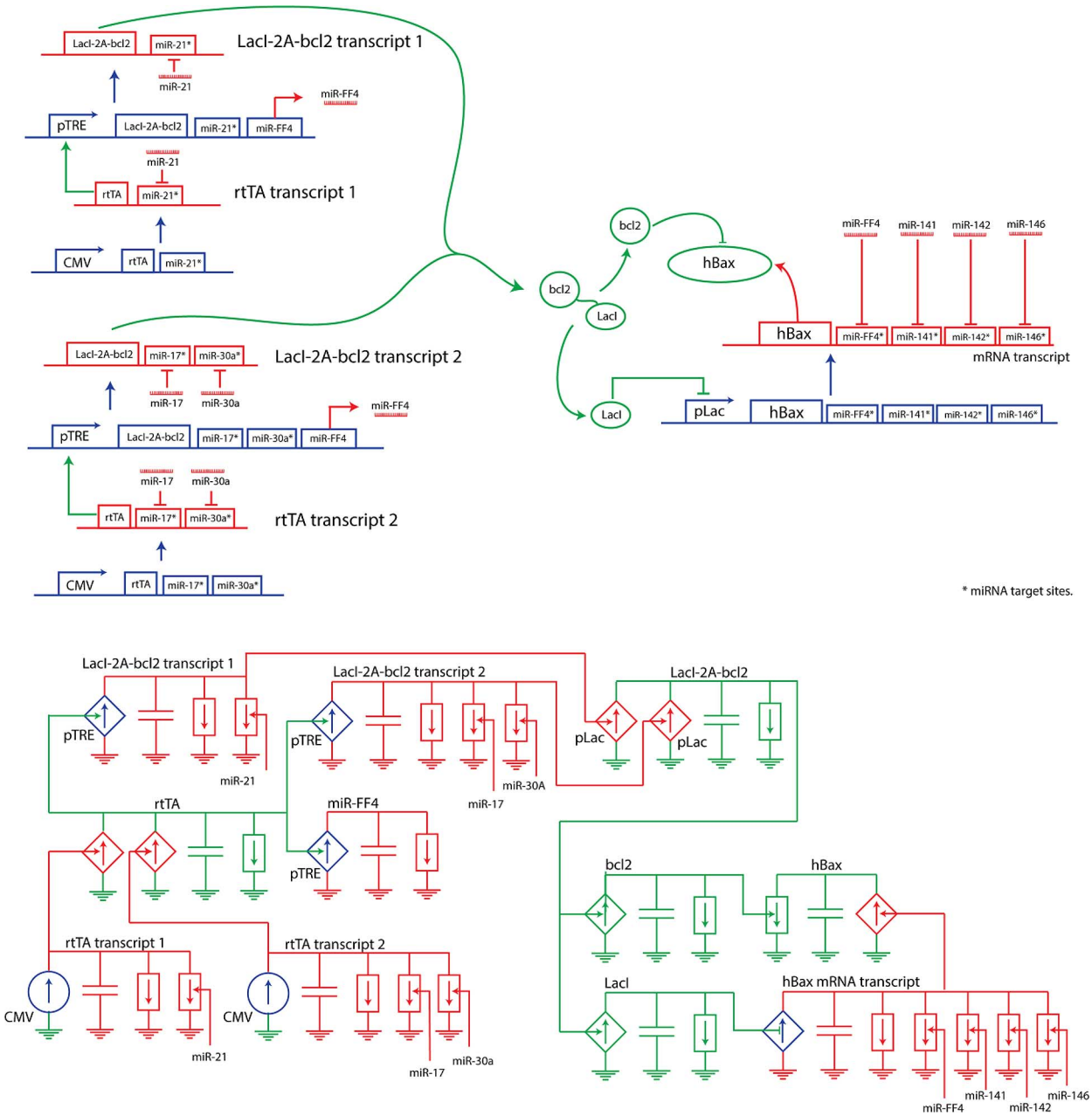

Fig. 14. A RNAi Logic Classifier Circuit [45]. At low levels of any HeLa-High markers (miR-21, (miR-17 + miR-30a)), bcl2 and LacI are co-translated via self-cleaving linker 2A. Once cleaved, LacI represses hBax expression while bcl2 inhibits hBax via protein binding. The additional repression provided by the synthetic miR-FF4 mRNA ensures that hBax concentration is low even under conditions that result in leaky hBax expression, as described in [45]. High levels of any HeLa-Low markers (miR-141,142,146) also reduce hBax expression by targeting the hBax mRNA transcript to the RNAi pathway. Overall, the circuit is an example of a 6-state-variable logic circuit implemented via highly redundant mechanisms described in the text.

base pairs with its target mRNA transcript. Once bound, RISC silences gene expression by one of several mechanisms, such as cleaving mRNA transcripts; promoting de-adenylation, which speeds up mRNA degradation; or by inhibiting translation initiation directly [43].

1) A RNAi Logic Classifier Circuit: In cells, miRNA is known to regulate cell cycle by repressing specific cyclin complexes [44]. The miRNA profiles in different cell types are often very different and reflect their differences in phenotype. Hence, miRNA is potentially a good biomarker to differentiate between cell types, in particular, between cancerous and normal cells. This idea was used in [45] to detect a six-variable miRNA profile characteristic of HeLa cervical cancer cells, and to express a suicide or apoptosis-promoting protein hBax, only upon successful detection of the profile. The key to designing an accurate classifier is to select miRNAs that are expressed at high or low levels in cancer cells, also known as HeLa-high or HeLa-low markers respectively, and to choose a sufficient number of markers such that the classifier has good selectivity without being overly complex. The logic in the circuit is configured such that HeLa-high miRNA markers, at high concentration, promote hBax expression, while HeLa-low miRNA markers effectively veto such expression if any of them are at high concentration. In [45], the strategy used was that

(miR_hi1, miR_hi2 + miR_hi3, miR_lo1, miR_lo2, miR_lo3) must be at (1, 1, 0, 0, 0) logic levels in order for the killing hBax protein to be expressed. In particular, the specific miRNAs in the HeLa cell that were used corresponding to the above logic were (miR-21, miR-17 + miR-30a, miR-141, miR-142(3p), miR-146a). The circuit that implements this logic along with a circuit schematic is shown in Fig. 14.

While the circuit of Fig. 14 appears to be fairly complex, it simplifies considerably if one realizes that a lot of its apparent complexity arises from its use of redundant logic. Such redundancy improves the effective on/off ratio, which is not high in most cells in a single logical stage, by repeating the same logic function with the same input(s) in a cascade of two stages to get a higher on/off ratio: the effective on/off ratio is then the product of the on/off ratios of the two logical stages in the cascade.

The basic logic of the circuit of Fig. 14 can be understood as follows: The LacI-bcl2 transcript 1 is generated if miR-21 is NOT 1; if it is, serial RNAi redundant logic will block the rtTA transcript 1 translation as well as LacI-2A-bcl2 transcript 1 translation in the two-logic-stage rtTA-LacI cascade. Similarly, the LacI-2A-bcl2 transcript 2 is generated via redundant logic if (miR-17 + miR-30a) is NOT 1 via similar serial redundant logic in a two-stage cascade. Note that both miR-17 and miR-30a must both NOT be 1 in order for rtTA translation to proceed, such that the needed (miR-17 + miR-30a) OR logic is naturally implemented via a dual AND version. Overall, the generation of the LacI-bcl2 transcripts, whether via transcript 1 or via transcript 2, both of which lead to identical LacI-bcl2 proteins implies that the HeLa-high conditions are not satisfied and that hBax production must be inactivated. To do so, the LacI-bcl2 protein self cleaves to implement redundant logic in a two-stage serial cascade, once via LacI repression of hBax generation, and once via bcl2-hBax protein binding, preventing its oligomerization [46]. Finally, the requirement that (miR-141, miR-142, miR-146) all be at 0 levels for hBax to be produced is implemented by having any of them block translation on the hBax mRNA transcript. This translational blocking is the only non-redundant logic in the entire circuit.

The final redundant two-stage logic circuit in Fig. 14, which has been neglected until now, arises from the synthetic miR-FF4 miRNA: Since it is always present whenever the LacI-bcl2 transcript is present, repression of hBax production is achieved via transcription repression by LacI as well as by translation repression by miR-FF4.

The analog circuit schematic of Fig. 14 sheds clarity on how the logic is implemented at the blue, red, or green levels. Furthermore, since actual implementations are not as digital as described, it allows one to represent how the various parameters such as degradation or actual on/off ratios, affect circuit operation. Future implementations of such a classifier could likely be improved by using analog pattern recognition circuits that are insensitive to absolute signal values in the miRNA patterns, which vary amongst cells, but are sensitive to the relative miRNA ratios that convey information about cell phenotype.

2) A Controlled Splicing Circuit: Splicing is another way of modifying RNA to regulate gene expression as shown in Fig. 5. It is the process of removing introns while joining exons from pre-RNA to form a spliced mRNA transcript. Splicing can be

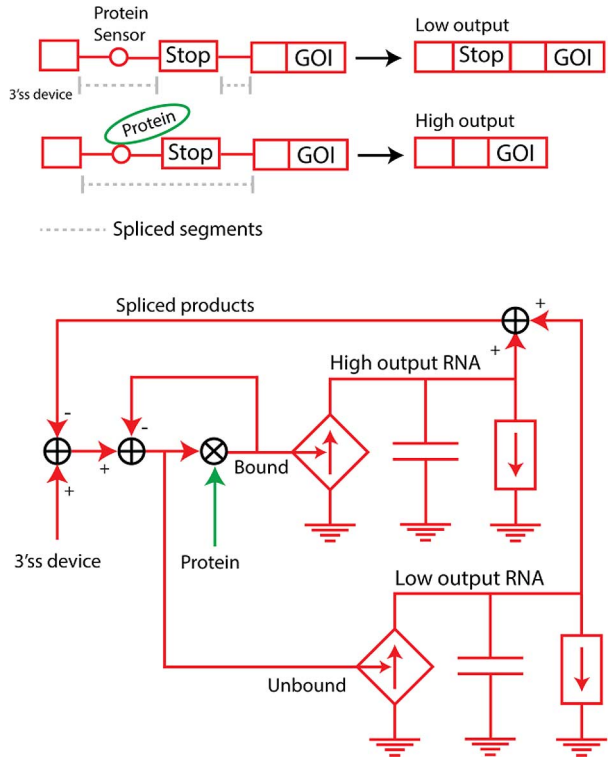

Fig. 15. A Controlled Splicing Circuit [52]. An aptamer is added to the intronic region next to the exon containing a stop codon. When the aptamer is not bound by a ligand, only the introns are spliced out, leaving a transcript with an upstream stop codon. This stop codon drastically reduces protein output. When a ligand is added, the RNA adopts a new conformation that blocks the intron-exon boundaries via steric hindrance, such that the intron-exon-intron sequence is spliced from the transcript. The final transcript is free from any premature stop codon, which then leads to high levels of gene expression.

used to design an RNA device that integrates a protein-binding aptamer in the intronic region of a mini-gene construct as shown in Fig. 15 [52]. In this case, the construct also encodes a stop codon, which is flanked by two introns. When placed upstream of a gene of interest, the mini-gene essentially adds a stop codon to the spliced transcript right next to the gene of interest, which results in pre-mature termination of translation. When a cognate protein binds to the aptamer, it alters the shape of the transcript and is thought to block the spliceosome recognition sites that flank the exon via steric hindrance. Consequently, the intron-exon-intron sequence is spliced from the transcript, which also removes the stop codon, and the resulting transcript now expresses the protein of interest. The analog circuit schematic in Fig. 15 reveals the usual use-it-and-lose-it feedback loops and the dynamics that govern this controlled splicing circuit.

3) A Translational Riboswitch: The formation of miRNA offers mechanistic strategies that can be used to regulate gene expression. In eukaryotic cells, miRNA is first transcribed by RNA polymerase II [53], and forms a nascent precursor molecule called pri-miRNA. Drosha, an RNase III enzyme, cleaves the pri-miRNA into ~70 nucleotide long pre-miRNA. Pre-miRNA takes on a stem-loop structure and is processed by yet another RNase III enzyme, Dicer. Finally, the mature miRNA is incorporated into RISC. Throughout the processing, non-essential fragments are trimmed from the precursor molecules and rapidly degraded. In theory, a synthetic gene

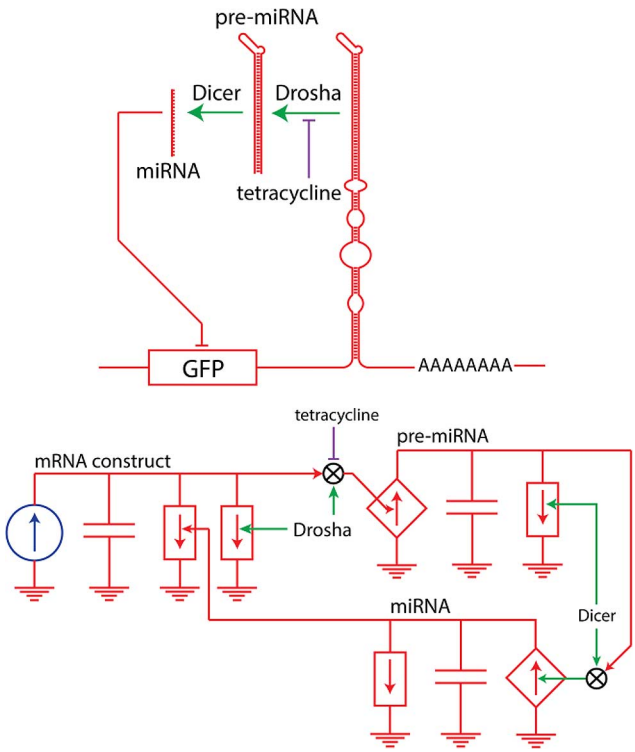

Fig. 16. A Translational Riboswitch [54]. The RNA device contains a GFP coding region, a tetracyline aptamer, a pri-miRNA with Drosha cleavage site and a poly-A tail. When the RNA is cleaved by Drosha, it loses its poly-A tail and is destabilized. In addition, the pre-miRNA from the cleavage is processed by Dicer into a mature miRNA which targets the GFP coding region on other RNAs. Overall, GFP is strongly repressed. In the presence of tetracycline, the aptamer adopts a structure that prevents Drosha from cleaving it, thus acting as a derepressor.

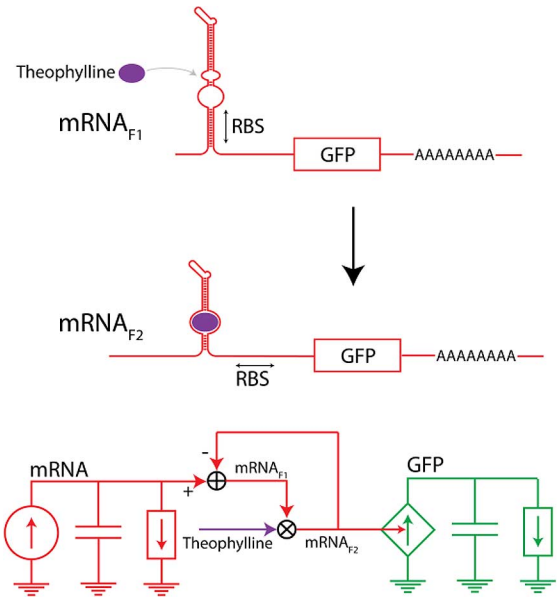

Fig. 17. A Theophylline-responsive Riboswitch [55]. The riboswitch uses an aptamer-based design. When Theophylline is added, the ribosome binding site (RBS) becomes exposed, which initiates translation.

could be regulated by miRNA-formation mechanisms if it is linked to a pri-miRNA was feasible: As Fig. 16 shows, a pri-miRNA sequence was encoded in the 3' UTR of an mRNA transcript coding for a protein of interest. Drosha processing cleaved out pre-miRNAs and separated the coding region from the poly-A tail, thereby promoting degradation of the fragments, and thus repressing gene expression. The resulting miRNA was complementary to the very transcript it was made from, so it also targeted other copies of the transcripts, effectively providing a second layer of repression.

Such an RNA device can also be converted to a riboswitch by encoding an aptamer within it, that is say, sensitive to a small molecule such as theophylline. Upon binding, the RNA-theophylline complex adopts a structured conformation that blocks Drosha processing, possibly via steric hindrance. As theophylline concentration changes, the circuit produces a graded response in gene expression; at high concentrations of theophylline, gene expression is high, and vice versa. In summary, by encoding a gene with a pri-miRNA sequence and with an RNA aptamer, a ligand-sensitive circuit capable of strong transcriptional repression was created. The analog circuit schematic shows the feedback loops that represent this molecular circuit.

4) A Theophylline-Responsive Riboswitch: When theophylline binds to an RNA aptamer, the RNA structural change has several other implications as well, such as exposing parts of the RNA that were previously sequestered via base pairing. An early riboswitch design used this mechanism as a way to control translation [55]. It first places the aptamer upstream of the Ribosome Binding Site (RBS). The RBS is initially inaccessible due to the extensive pairwise interactions it forms with the 5'UTR. When the aptamer is activated by theophylline, it adopts a different structure, which exposes the RBS for translation initiation as shown in Fig. 17. The analog circuit schematic that represents the riboswitch is shown.

5) A ncRNA-Responsive Riboswitch: pT181, a trans-acting ncRNA, can also be used to regulate riboswitches [56]. Like theophylline, Fig. 18 shows that pT181 targets the 5' UTR of the mRNA transcript and blocks transcription when bound to the mRNA. Mechanistically, pT181 binds to the terminator hairpin in the 5' UTR and stabilizes it. The presence of the hairpin stalls RNA polymerase, which results in the early termination of transcription. In the absence of pT181, an anti-terminator loop is formed and transcription proceeds. Using an ncRNA regulator implies that the specificity and repression efficiency of the ncRNA may be tuned finely, making a highly modular regulatory device feasible. The analog circuit schematic for this device is shown.

6) CRISPR Circuits: A CRISPR (Clustered Regularly Interspaced Short Palindromic Repeats)-Cas system has been adapted to perform transcriptional interference, drawing several parallels to the RNAi pathway [57]. Cas9, a DNA endonuclease, recruits a small guide RNA (sgRNA) as a template for double stranded DNA (dsDNA) recognition. The resulting complex will bind to any DNA that is complementary to the embedded sgRNA and cleave it. This mechanism is analogous to miRNA-based translational repression, wherein RISC uses miRNA as a guide RNA to find and cleave its target.

Due to the high specificity of CRISPR-Cas9, it has provided an excellent tool for genome editing [58]. For applications that

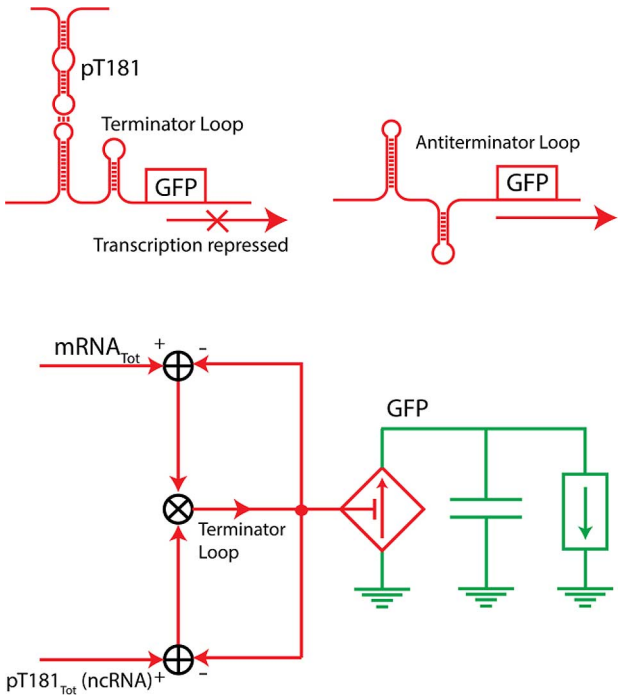

Fig. 18. A ncRNA-responsive Riboswitch [56]. Transcription is regulated by pT181, which induces the formation of a transcription terminator hairpin in the 5' UTR region. This hairpin triggers the premature dissociation of RNA polymerase, thus repressing transcription. In the absence of pT181, the 5' UTR region adopts an anti-terminator hairpin conformation instead and transcription proceeds as normal.

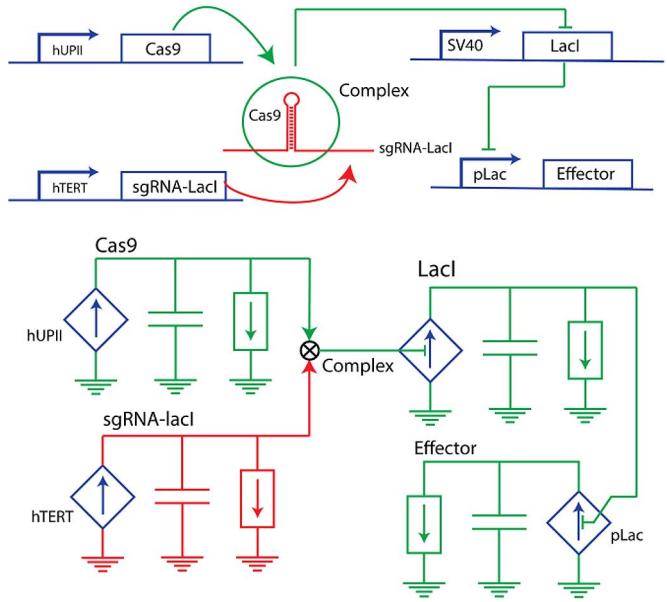

Fig. 19. An 'AND' Logic CRISPR Circuit [60]. When transfected into bladder cancer cells, cancer-specific promoter hTERT and bladder-specific promoter hUP II will drive sgRNA-LacI and Cas9 respectively. The resulting Cas9-sgRNA complex binds and cleaves the DNA sequence of LacI gene specifically, thus reducing LacI expression. At low concentrations of LacI, the effector is successfully expressed.

do not benefit from editing the genome, but desire specific regulation, a mutated Cas9 (dCas9), with a DNA binding domain but no nuclease activity can efficiently implement steric blocking of transcription: A CRISPR interference system (CRISPRi) that uses dCas9 and sgRNA was able to repress transcription efficiency by up to 1000-fold [59]. By designing dCas9 and sgRNA to target inducible promoters, the level of repression can be controlled as well. Several labs have demonstrated the use of CRISPRi pathway in designing a variety of biological circuits, such as logic gates in Fig. 19 [60], and layered signaling cascades [61], [62].

The analog circuit schematic in Fig. 19 clearly illustrates how the combination of protein (Cas9) and RNA (sgRNA-LacI), which form a complex, reduces the production of LacI, and thus increases the expression of the effector protein.

C. Protein-Based Circuits

1) A TEV-Protease Receptor Circuit: Changes in protein conformation and binding occur at a much faster time scale than the processes of transcription and translation such that protein circuits offer significantly faster response times [63], [64]. Protein specificity and function can also be modified through mutagenesis or fusion enabling flexibility. Fig. 20 shows how fusion proteins can also be used as an assay for receptor activation [65]: The receptor is joined to a transcription factor via a tether that contains the tobacco etch virus (TEV) protease cleavage site. When activated by a ligand, the receptor recruits a cognate arrestin protein, which is fused with the TEV protease. The protease cleaves the tether upon binding such that the transcription

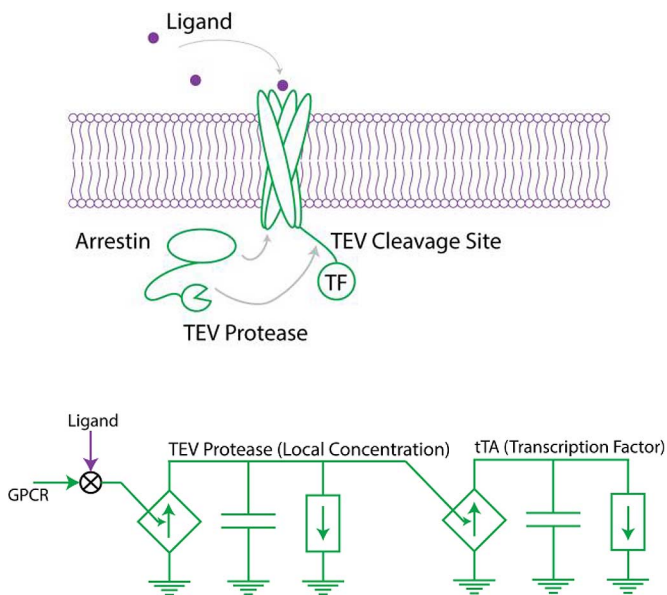

Fig. 20. A TEV-Protease Receptor Circuit [65]. Upon binding of ligand, the GPCR receptor recruits the arrestin-TEV-protease fusion protein. The TEV protease cleaves the tether between the GPCR receptor and transcription factor (TF) and releases the TF into the cytoplasm. The TF may then activate other transcription circuits.

factor is released, thus activating gene expression. The analog circuit schematic is a classic two-gain-stage amplifying cascade that saturates at large input ligand levels.

2) A Protein Multiplier Circuit: Nissim and Bar-Ziv used fusion proteins to construct a dual-promoter expression integrator (DPI) [66], which can effectively implement multiplication or an AND logic function with protein circuits. The circuit is shown in Fig. 21. One of the two proteins has a yeast GAL4

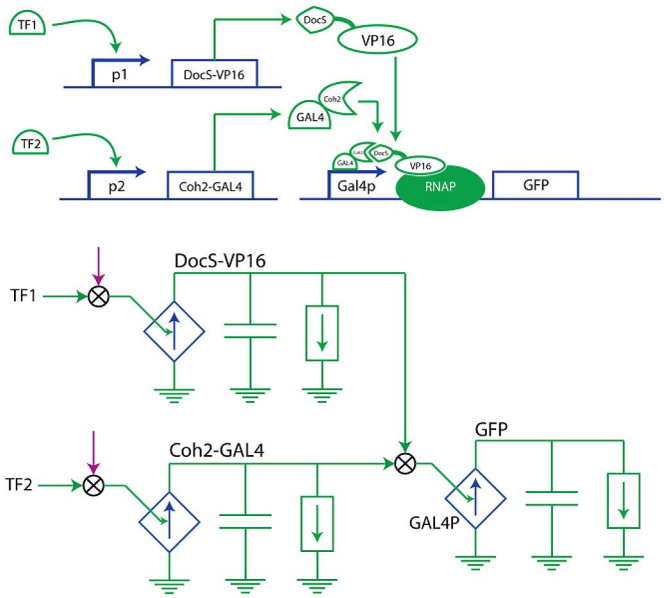

Fig. 21. A Protein Multiplier Circuit [67]. Inputs TF1 and TF2 drive the expression of fusion proteins DocS-VP16 and Coh2-GAL4. GAL4 first binds to its cognate promoter and recruits VP16 via the tight binding of DocS and Coh2. VP16 then drives the expression of GFP. If either TF1 or TF2 is absent, GFP output will remain low.

DNA binding domain that is fused with bacterial protein Cohesion (Coh2). The second protein has a Dockerin (DocS) domain fused to a VP16 domain, a strong transcription-activating domain. Coh2 and DocS bind with high affinity [67], and their association brings both GAL4 and VP16 into close proximity of each other. Together, the resulting complex exhibits strong transcriptional activation capabilities, similar to a GAL4-VP16 fusion protein [68]. By placing Coh2-GAL4 and DocS-VP16 genes downstream of inducible promoters, the circuit expresses its output only when both fusion proteins are expressed. The equivalent analog circuit schematic is also shown in Fig. 21.

3) Dynamical Protein Circuits: In the protein circuits discussed thus far, the domains that make up a fusion protein are typically fixed once the gene encoding it has been designed. It is possible to construct a fusion protein that can be altered dynamically such that it acquires different functional domains depending on varying conditions within the cell. This modification leads to a class of protein-based devices that can respond quickly to changing environments.

Fig. 22 shows the protein scaffold Ste5 along with the Msg5 modulator protein. This Ste5 scaffold binds to Ste11, Ste7 and Fus3, three kinases that phosphorylate one another in sequence and thus create an amplifying cascade of phosphorylation in this portion of the 'MAPK pathway' [5]. Msg5 is a phosphatase that dephosphorylates Fus3, thus reducing MAPK pathway output and serving as a negative modulator of the kinase amplifying cascade housed by Ste5 [70]; in contrast, Ste50 activates Ste11, increases MAPK pathway output and is a positive modulator of the kinase amplifying cascade housed by Ste5 [71]. Fig. 22 shows that because negative-modulator output is controlled by the MAPK pathway and vice versa, a negative-feedback loop can be designed to architect dynamic functions. Similarly, positive modulators can implement positive-feedback loops.

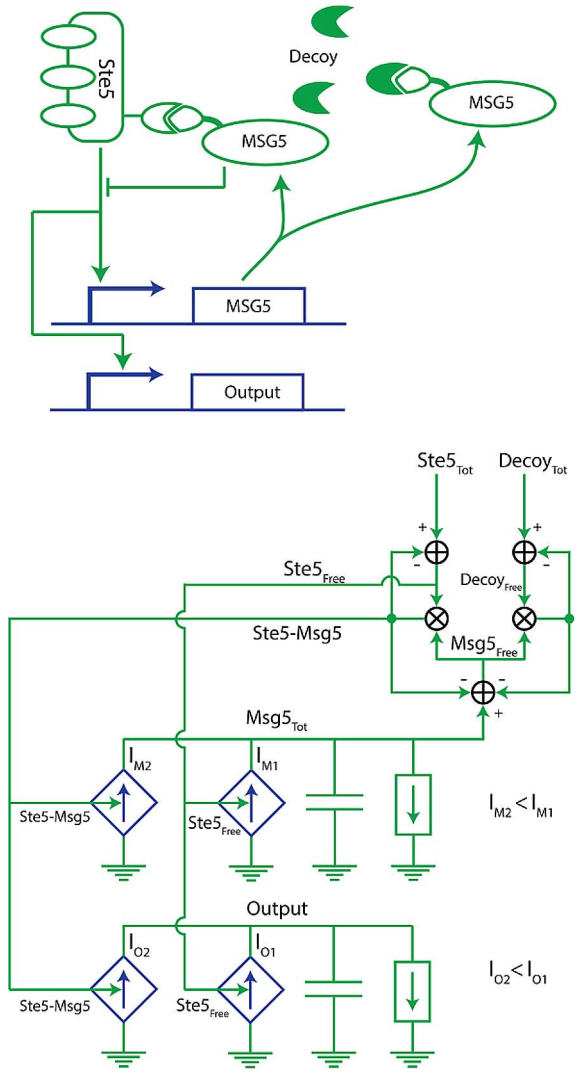

Fig. 22. Dynamical Protein Circuits [69]. *Components.* Ste5 is a protein scaffold that binds to Ste11, Ste7 and Fus3, three kinases that phosphorylate one another in sequence. Msg5 is a MAPK phosphatase that inactivates phosphorylated Fus3. Both Ste5 and Msg5 are modified to include complementary leucine zipper sites, which allow Msg5 to associate with Ste5 and negatively modulate its kinase amplifying cascade activity. In this pulse-generator example circuit, Ste5 activates the signaling cascade that leads to the expression of modified Msg5. Normally, Msg5 would inhibit the cascade, completing the negative feedback loop, but the presence of the decoy zipper that binds with higher affinity shunts Msg5 away from Ste5. Only when Msg5 saturates the entire available Decoy will it bind to Ste5 to inhibit its activity. These dynamics lead to the generation of a pulse.

In Fig. 22, Ste5 activates the signaling cascade that leads to the expression of modified Msg5. Normally, Msg5 would inhibit the cascade, completing the negative feedback loop, but the presence of a decoy protein that binds Msg5 with higher affinity directs Msg5 away from Ste5. Only when Msg5 saturates all the available Decoy proteins, will it bind to Ste5 to inhibit its activity. Therefore, in response to an input to Ste5, a pulse is generated: The Fus3 output remains high until sufficient Msg5, unbound to Decoy, is created after which the activity of Fus3 can be turned down.

The analog circuit schematic that represents the circuit is also shown in Fig. 22. The negative-feedback loop due to Msg5 explains why a pulse is generated: Delayed negative feedback al-

ways causes a derivative response, which in this case leads to a pulse. The use-it-and-lose-it feedback loops model loading effects that may be significant at low molecular count. Linear and non-linear dynamics due to positive and negative-feedback loops, and their stochastic behavior due to low molecular counts at the Ste5 input may be represented as needed.

IV. Resource Consumption

The previous sections have reviewed several specific circuits that operate at the DNA, RNA, protein, and small-molecule levels via the lens of analog circuits. It is now time to step back from the details and review a few fundamental principles that determine the scaling behavior of these circuits.

The fundamental laws of noise in gene and protein expression [19] set limits on the energy, time, space, molecular count, and part-count resources needed to compute at a given level of precision [4]. Using these laws for the fundamental genetic circuit represented in Fig. 4, it has been shown that the molecular counts of protein and RNA, N_{prot} and N_{mRNA}, and power consumption, P_{prot}, required to represent a protein output at a given signal-to-noise ratio, S_N, and at a given protein degradation bandwidth, $1/\tau$, are given by

$$\begin{aligned} N_{\mathrm{prot}} &= (\beta_{\mathrm{eff}} + 1) S_N \\ N_{\mathrm{mRNA}} &= \frac{N_{\mathrm{prot}}}{A_v} \\ P_{\mathrm{prot}} &= \frac{S_N}{\tau_{\mathrm{prot}}} (\beta_{\mathrm{eff}} + 1) \left(\frac{E_{\mathrm{mRNA}}}{\beta_{\mathrm{eff}}} + E_{\mathrm{prot}} \right) \end{aligned} \tag{6}$$

where β_{eff} is a 'burst-noise factor' parameter [3], [19], [29], A_v is the protein to mRNA copy-number ratio, and E_{mRNA} and E_{prot} are the ATP costs of synthesizing an mRNA or a protein. Thus, for any given biological circuit design we can map the resource consumption rate of ATP to P_{prot} and the molecular-copy-number resource use to an analog voltage N_{prot}.

Using the resource-precision equations of (6), work in [4] has shown that analog computation is significantly more efficient than digital computation at the modest 2-to-5-bit precision in cells w.r.t. the use of molecular copy number, ATP consumption, and in general, w.r.t. the use of all cellular machinery. Fig. 23 was computed for the simple exemplary computation of addition in yeast for the two resources of molecular copy number [Fig. 23(a)] and ATP power consumption [Fig. 23(b)] [4]. Work in [3], [77] has shown that cells must use collective analog strategies to be scalable and efficient in their use of resources. Collective analog computation is scalable to arbitrary complexity and precision using many moderate-precision analog parts that collectively interact via analog and digital means as in the brain. For example, recent work showed how to create a 16-bit-precise adder on a working experimental chip using four interacting 4-bit-precise analog units [78]. These units computed using the analog basis function of Kirchhoff's current law rather than logic and used discrete event-based interactions amongst the analog units. Similarly, by using state-machines, e.g., like those with recombinases that are discussed in [73]–[75], molecular circuits that do arbitrarily complex sequential analog computation can be built in a hybrid state machine configuration [3], [84]. In terms of robustness and efficiency, such state machines exploit the best of the analog and digital domains [3], [77], [84] and are easily capable of being programmed [81], [84] to do universal Turing computation.

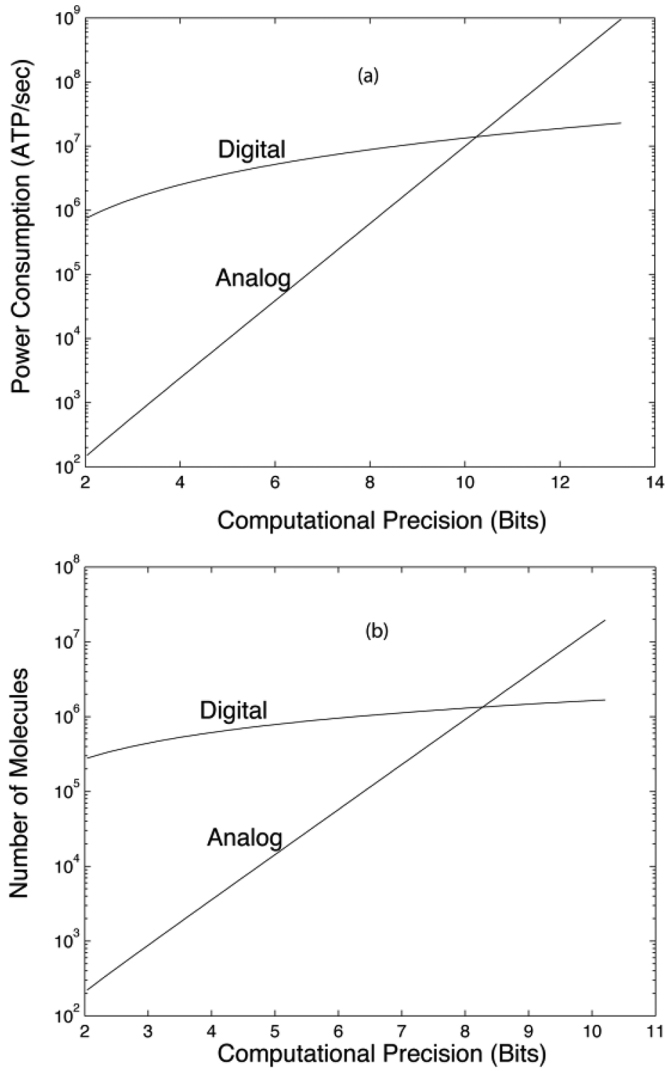

Fig. 23. The Costs of Analog versus Digital Computation [4]. The graph shows (a) the power consumption and; (b) the number of molecules needed for analog or digital genetic adders over varying levels of computational precision.

Due to the shared use of ribosomes, polymerases, RNAases, proteases, and ATP amongst several protein-synthesizing synthetic circuits, 'cross talk' interactions amongst these circuits can occur. Such cross talk is easily represented via adder interactions as in Figs. 3 or 10 or via Kirchhoff's current law in cytomorphic circuits [3], [76]. Such representations show the ubiquitous presence of use-it-and-lose-it feedback loops in biological computation, which in turn lead to the ubiquitous importance of non-modularity and loading.

V. Conclusion

In the past, the synergy between circuits in biology and circuits in electronics has led to productive research in neurobiological systems in the eye, ear, vocal tract, heart, and brain, for example as described in [31], [78]–[90]. However, the deep mathematical similarity captured by Fig. 2 and (2)

including stochastics make analog circuits and analog cytomorphic transistor circuits especially powerful for design, analysis, simulation, and implementation of synthetic biological circuits: robustness-efficiency, analog-digital, and other feedback-circuits-and-systems tradeoffs in cells are identical to those in ultra-low-power analog circuit design [3], [4]. Ultra-low-power analog electronic circuits face very similar tradeoffs like cells in biology because of their need to operate quickly, accurately and robustly in spite of mismatched and noisy components and signals, a necessary consequence of having very low levels of available power and space or parts. A review of over 17 circuits in this paper over two decades and the canonical circuit of Fig. 5 suggest that analog circuits, a relatively mature discipline, may provide a unifying and useful intuitive-and-rigorous language for helping synthetic biology, a relatively modern discipline, scale. Indeed there is an increasing appreciation in the synthetic-biology community of the importance of analog circuits and analog computation for the future of the field [91].

REFERENCES

[1] P. E. M. Purnick and R. Weiss, "The second wave of synthetic biology: From modules to systems," *Nat. Rev. Mol. Cell. Biol.*, vol. 10, pp. 410–422, Jun. 2009.

[2] T. S. Moon, C. Lou, A. Tamsir, B. C. Stanton, and C. A. Voigt, "Genetic programs constructed from layered logic gates in single cells," *Nature*, vol. 491, pp. 249–253, Nov. 2012.

[3] R. Sarpeshkar, "Cytomorphic electronics: Cell-inspired electronics for synthetic and systems biology," in *Ultra Low Power Bioelectronics: Fundamentals, Biomedical Applications, and Bio-Inspired Systems*. Cambridge, U.K.: Cambridge Univ. Press, Feb. 2010, ch. 24 (chapters 2, 7, 8, 9, 10 on feedback systems and noise may also be useful) [Online]. Available: http://www.rle.mit.edu/acbs/publications; http://www.rle.mit.edu/acbs/wp-content/uploads/2014/03/ULPB_2010_bkprvw.pdf

[4] R. Sarpeshkar, "Analog synthetic biology," *Philos. Trans. Roy. Soc. London A* vol. 372, p. 20130110, 2014 [Online]. Available: http://dx.doi.org/10.1098/rsta.2013.0110

[5] H. Lodish, A. Berk, C. A. Kaiser, M. Krieger, M. P. Scott, A. Bretscher, H. Ploegh, and P. Matsudaira, *Molecular Cell Biology*, 6th ed. San Francisco, CA, USA: Freeman, 2008.

[6] V. V. Zhirnov and R. K. Cavin, "Future microsystems for information processing: Limits and lessons from the living systems," *IEEE J. Electron Devices Soc.*, vol. 1, pp. 29–47, 2013.

[7] R. Daniel, J. R. Rubens, R. Sarpeshkar, and T. K. Lu, "Synthetic analog computation in living cells," *Nature* vol. 497, pp. 619–623, May 30, 2013, doi:10.1038/nature12148.

[8] D. Del Vecchio, A. J. Ninfa, and E. D. Sontag, "Modular cell biology: Retroactivity and insulation," *Mol. Syst. Biol.*, vol. 4, p. 161, 2008.

[9] K. S. Nilgiriwala, J. Jiménez, P. M. Rivera, and D. Del Vecchio, "Synthetic tunable amplifying buffer circuit in *E. coli*," *ACS Synth. Biol.*, Oct. 2014.

[10] S. Cardinale and A. P. Arkin, "Contextualizing context for synthetic biology: Identifying causes of failure of synthetic biological systems," *Biotechnol. J.*, vol. 7, pp. 856–866, Jul. 2012.

[11] U. Moran, R. Phillips, and R. Milo, "SnapShot: Key numbers in biology," *Cell*, vol. 141, pp. 1262–1262.e1, Jun. 2010.

[12] R. Milo and R. Phillips, "Cell biology by the numbers," Book Draft, Personal Communication From Authors Jun. 2014.

[13] A. Wagner, "Energy constraints on the evolution of gene expression," *Mol. Biol. Evol.*, vol. 22, pp. 1365–1374, Jun. 2005.

[14] J. Vind, M. A. Sørensen, M. D. Rasmussen, and S. Pedersen, "Synthesis of proteins in Escherichia coli is limited by the concentration of free ribosomes. Expression from reporter genes does not always reflect functional mRNA levels," *J Mol. Biol.*, vol. 231, pp. 678–688, Jun. 1993.

[15] W. E. Bentley, N. Mirjalili, D. C. Andersen, R. H. Davis, and D. S. Kompala, "Plasmid-encoded protein: The principal factor in the "metabolic burden" associated with recombinant bacteria," *Biotechnol. Bioeng.*, vol. 35, pp. 668–681, Mar. 1990.

[16] N. A. Cookson, W. H. Mather, T. Danino, O. Mondragón-Palomino, R. J. Williams, L. S. Tsimring, and J. Hasty, "Queueing up for enzymatic processing: Correlated signaling through coupled degradation," *Mol. Syst. Biol.*, vol. 7, p. 561, 2011.

[17] D. De Vos, F. J. Bruggeman, H. V. Westerhoff, and B. M. Bakker, "How molecular competition influences fluxes in gene expression networks," *PLoS One*, vol. 6, p. e28494, 2011.

[18] A. Prindle, J. Selimkhanov, H. Li, I. Razinkov, L. S. Tsimring, and J. Hasty, "Rapid and tunable post-translational coupling of genetic circuits," *Nature*, vol. 508, pp. 387–391, Apr. 2014.

[19] E. M. Ozbudak, M. Thattai, I. Kurtser, A. D. Grossman, and A. van Oudenaarden, "Regulation of noise in the expression of a single gene," *Nature Genet.*, vol. 31, pp. 69–73, May 2002.

[20] D. T. Gillespie, "Exact stochastic simulation of coupled chemical reactions," *Abstr. Pap. Amer. Chem. Soc.*, vol. 173, pp. 128–128, 1977.

[21] M. A. Gibson and J. Bruck, "Efficient exact stochastic simulation of chemical systems with many species and many channels," *J. Phys. Chem. A*, vol. 104, pp. 1876–1889, Mar. 2000.

[22] D. T. Gillespie, "Approximate accelerated stochastic simulation of chemically reacting systems," *J. Chem. Phys.*, vol. 115, pp. 1716–1733, Jul. 2001.

[23] M. Schwehm, "Parallel stochastic simulation of whole-cell models," in *Proc. 2nd Int. Conf. Systems Biology*, 2001, pp. 333–341.

[24] J. R. Karr, J. C. Sanghvi, D. N. Macklin, M. V. Gutschow, J. M. Jacobs, B. Bolival, Jr., N. Assad-Garcia, J. I. Glass, and M. W. Covert, "A whole-cell computational model predicts phenotype from genotype," *Cell*, vol. 150, pp. 389–401, Jul. 2012.

[25] S. L. Spencer, S. Gaudet, J. G. Albeck, J. M. Burke, and P. K. Sorger, "Non-genetic origins of cell-to-cell variability in TRAIL-induced apoptosis," *Nature*, vol. 459, pp. 428–432, May 2009.

[26] K. Lewis, S. Gottesman, and C. S. Harwood, "Persister cells," *Annu. Rev. Microbiol.*, vol. 64, pp. 357–372, 2010.

[27] R. Daniel, S. S. Woo, L. Turicchia, and R. Sarpeshkar, "Analog transistor models of bacterial genetic circuits," in *Proc. IEEE Biological Circuits and Systems Conf.*, San Diego, CA, USA, Jun. 2011, pp. 333–336.

[28] S. Mandal and R. Sarpeshkar, "Log domain circuit models of chemical reactions," in *Proc. IEEE Int. Synp. Circuits and Systems*, May 2009, pp. 2697–2700.

[29] S. Mandal and R. Sarpeshkar, "Circuit models of stochastic genetic networks," in *Proc. IEEE Symp. Biological Circuits and Systems*, Beijing, China, Nov. 2009, pp. 109–112.

[30] K. H. Wee, L. Turicchia, and R. Sarpeshkar, "An analog integrated-circuit vocal tract," *IEEE Trans. Biomed. Circuits Syst.*, vol. 2, pp. 316–327, Dec. 2008.

[31] K. H. Wee, L. Turicchia, and R. Sarpeshkar, "An articulatory silicon vocal tract for speech and hearing prostheses," *IEEE Trans. Biomed. Circuits Syst.*, vol. 5, no. 4, pp. 339–346, Aug. 2011.

[32] T. S. Gardner, C. R. Cantor, and J. J. Collins, "Construction of a genetic toggle switch in Escherichia coli," *Nature*, vol. 403, pp. 339–342, Jan. 2000.

[33] W. Sha, J. Moore, K. Chen, A. D. Lassaletta, C.-S. Yi, J. J. Tyson, and J. C. Sible, "Hysteresis drives cell-cycle transitions in Xenopus laevis egg extracts," *Proc. Nat. Acad. Sci. USA*, vol. 100, pp. 975–980, Feb. 2003.

[34] A. Chen, A. Sanchez, L. Dai, and J. Gore, "Dynamics of a producer-freeloader ecosystem on the brink of collapse," *Nat. Commun.*, vol. 5, May 2014.

[35] B. P. Kramer and M. Fussenegger, "Hysteresis in a synthetic mammalian gene network," *Proc. Nat. Acad. Sci. USA*, vol. 102, pp. 9517–9522, 2005.

[36] M. J. Berridge, M. D. Bootman, and P. Lipp, "Calcium—A life and death signal," *Nature*, vol. 395, pp. 645–648, Oct. 1998.

[37] C. S. Pittendrigh, "Temporal organization: Reflections of a Darwinian clock-watcher," *Annu. Rev. Physiol.*, vol. 55, pp. 16–54, 1993.

[38] A. M. Turing, "The chemical basis of morphogenesis," *Bull. Math. Biol.*, vol. 52, pp. 153–197, 1990.

[39] M. B. Elowitz and S. Leibler, "A synthetic oscillatory network of transcriptional regulators," *Nature*, vol. 403, pp. 335–338, Jan. 2000.

[40] J. Stricker, S. Cookson, M. R. Bennett, W. H. Mather, L. S. Tsimring, and J. Hasty, "A fast, robust and tunable synthetic gene oscillator," *Nature*, vol. 456, pp. 516–519, Nov. 2008.

[41] S. Basu, Y. Gerchman, C. H. Collins, F. H. Arnold, and R. Weiss, "A synthetic multicellular system for programmed pattern formation," *Nature*, vol. 434, pp. 1130–1134, Apr. 2005.

[42] L. S. Qi and A. P. Arkin, "A versatile framework for microbial engineering using synthetic non-coding RNAs," *Nat. Rev. Microbiol.*, vol. 12, pp. 341–354, May 2014.

[43] S. Rüegger and H. Großhans, "MicroRNA turnover: When, how, and why," *Trends Biochem. Sci.*, vol. 37, pp. 436–446, Oct. 2012.

[44] M. J. Bueno and M. Malumbres, "MicroRNAs and the cell cycle," *Biochim. Biophys. Acta-Mol. Basis Dis.*, vol. 1812, pp. 592–601, May 2011.

[45] Z. Xie, L. Wroblewska, L. Prochazka, R. Weiss, and Y. Benenson, "Multi-input RNAi-based logic circuit for identification of specific cancer cells," *Science*, vol. 333, pp. 1307–1311, Sep. 2011.

[46] J. Ding, Z. Zhang, G. J. Roberts, M. Falcone, Y. Miao, Y. Shao, X. C. Zhang, D. W. Andrews, and J. Lin, "Bcl-2 and Bax interact via the BH1-3 groove-BH3 motif interface and a novel interface involving the BH4 motif," *J. Biol. Chem.*, vol. 285, pp. 28749–28763, Sep. 2010.

[47] B. Yurke and A. P. M. , Jr., "Using {DNA} to power nanostructures," *Genetic Program. Evolvable Mach.*, vol. 4, pp. 111–122, 2003.

[48] B. Yurke, A. J. Turberfield, A. P. Mills, Jr., F. C. Simmel, and J. L. Neumann, "A DNA-fuelled molecular machine made of DNA," *Nature*, vol. 406, pp. 605–608, Aug. 2000.

[49] G. Seelig, D. Soloveichik, D. Y. Zhang, and E. Winfree, "Enzyme-free nucleic acid logic circuits," *Science*, vol. 314, pp. 1585–1588, Dec. 2006.

[50] L. Qian, E. Winfree, and J. Bruck, "Neural network computation with DNA strand displacement cascades," *Nature*, vol. 475, pp. 368–372, Jul. 2011.

[51] S. Bhadra and A. D. Ellington, "Design and application of cotranscriptional non-enzymatic RNA circuits and signal transducers," *Nucleic Acids Res.*, vol. 42, p. e58, Apr. 2014.

[52] S. J. Culler, K. G. Hoff, and C. D. Smolke, "Reprogramming cellular behavior with RNA controllers responsive to endogenous proteins," *Science*, vol. 330, pp. 1251–1255, Nov. 2010.

[53] Y. Lee, M. Kim, J. J. Han, K. H. Yeom, S. Lee, S. H. Baek, and V. N. Kim, "MicroRNA genes are transcribed by RNA polymerase II," *Embo J.*, vol. 23, pp. 4051–4060, Oct. 2004.

[54] C. L. Beisel, Y. Y. Chen, S. J. Culler, K. G. Hoff, and C. D. Smolke, "Design of small molecule-responsive microRNAs based on structural requirements for Drosha processing," *Nucleic Acids Res.*, vol. 39, pp. 2981–2994, Apr. 2011.

[55] S. Topp and J. P. Gallivan, "Riboswitches in unexpected places-a synthetic riboswitch in a protein coding region," *RNA*, vol. 14, pp. 2498–2503, Dec. 2008.

[56] J. B. Lucks, L. Qi, V. K. Mutalik, D. Wang, and A. P. Arkin, "Versatile RNA-sensing transcriptional regulators for engineering genetic networks," *Proc. Nat. Acad. Sci. USA*, vol. 108, pp. 8617–8622, May 2011.

[57] F. A. Ran, P. D. Hsu, J. Wright, V. Agarwala, D. A. Scott, and F. Zhang, "Genome engineering using the CRISPR-Cas9 system," *Nat. Protoc.*, vol. 8, pp. 2281–2308, Nov. 2013.

[58] P. D. Hsu, E. S. Lander, and F. Zhang, "Development and applications of CRISPR-Cas9 for genome engineering," *Cell*, vol. 157, pp. 1262–1278, Jun. 2014.

[59] L. S. Qi, M. H. Larson, L. A. Gilbert, J. A. Doudna, J. S. Weissman, A. P. Arkin, and W. A. Lim, "Repurposing CRISPR as an RNA-guided platform for sequence-specific control of gene expression," *Cell*, vol. 152, pp. 1173–1183, Feb. 2013.

[60] Y. Liu, Y. Zeng, L. Liu, C. Zhuang, X. Fu, W. Huang, and Z. Cai, "Synthesizing AND gate genetic circuits based on CRISPR-Cas9 for identification of bladder cancer cells," *Nat. Commun.*, vol. 5, p. 5393, 2014.

[61] S. Kiani, J. Beal, M. R. Ebrahimkhani, J. Huh, R. N. Hall, Z. Xie, Y. Li, and R. Weiss, "CRISPR transcriptional repression devices and layered circuits in mammalian cells," *Nat. Methods*, vol. 11, pp. 723–726, Jul. 2014.

[62] L. Nissim, S. D. Perli, A. Fridkin, P. Perez-Pinera, and T. K. Lu, "Multiplexed and programmable regulation of gene networks with an integrated RNA and CRISPR/Cas toolkit in human cells," *Mol. Cell*, vol. 54, pp. 698–710, May 2014.

[63] J. Kubelka, J. Hofrichter, and W. A. Eaton, "The protein folding 'speed limit'," *Curr. Opin. Struct. Biol.*, vol. 14, pp. 76–88, Feb. 2004.

[64] D. Holcman and Z. Schuss, "Time scale of diffusion in molecular and cellular biology," *J. Phys. A, Math. Theor.*, vol. 47, May 2014.

[65] G. Barnea, W. Strapps, G. Herrada, Y. Berman, J. Ong, B. Kloss, R. Axel, and K. J. Lee, "The genetic design of signaling cascades to record receptor activation," *Proc. Nat. Acad. Sci. USA*, vol. 105, pp. 64–69, Jan. 2008.

[66] L. Nissim and R. H. Bar-Ziv, "A tunable dual-promoter integrator for targeting of cancer cells," *Mol. Syst. Biol.*, vol. 6, p. 444, Dec. 2010.

[67] Y. Barak, T. Handelsman, D. Nakar, A. Mechaly, R. Lamed, Y. Shoham, and E. A. Bayer, "Matching fusion protein systems for affinity analysis of two interacting families of proteins: The cohesin-dockerin interaction," *J. Mol. Recognit.*, vol. 18, pp. 491–501, 2005.

[68] I. Sadowski, J. Ma, S. Triezenberg, and M. Ptashne, "GAL4-VP16 is an unusually potent transcriptional activator," *Nature*, vol. 335, pp. 563–564, Oct. 1988.

[69] C. J. Bashor, N. C. Helman, S. Yan, and W. A. Lim, "Using engineered scaffold interactions to reshape MAP kinase pathway signaling dynamics," *Science*, vol. 319, pp. 1539–1543, Mar. 2008.

[70] X. L. Zhan, R. J. Deschenes, and K. L. Guan, "Differential regulation of FUS3 MAP kinase by tyrosine-specific phosphatases PTP2/PTP3 and dual-specificity phosphatase MSG5 in Saccharomyces cerevisiae," *Genes Dev.*, vol. 11, pp. 1690–1702, Jul. 1997.

[71] C. Wu, M. Arcand, G. Jansen, M. Zhong, T. Iouk, D. Y. Thomas, S. Meloche, and M. Whiteway, "Phosphorylation of the MAPKKK regulator Ste50p in Saccharomyces cerevisiae: A casein kinase I phosphorylation site is required for proper mating function," *Eukaryot Cell*, vol. 2, pp. 949–961, Oct. 2003.

[72] M. Tavakoli and R. Sarpeshkar, "A sinh resistor and its application to tanh linearization," *IEEE J. Solid-State Circuits*, vol. 40, pp. 536–543, Feb. 2005.

[73] D. M. Wolf, L. Fontaine-Bodin, I. Bischofs, G. Price, J. Keasling, and A. P. Arkin, "Memory in microbes: Quantifying history-dependent behavior in a bacterium," *PLoS One*, vol. 3, Feb. 2008.

[74] C. Yang, M. W. Tibbitt, L. Basta, and K. S. Anseth, "Mechanical memory and dosing influence stem cell fate," *Nat. Mater.*, vol. 13, pp. 645–652, Jun. 2014.

[75] T. S. Ham, S. K. Lee, J. D. Keasling, and A. P. Arkin, "Design and construction of a double inversion recombination switch for heritable sequential genetic memory," *PLoS One*, vol. 3, p. e2815, 2008.

[76] S. S. Woo, J. Kim, and R. Sarpeshkar, "A cytomorphic chip for quantitative modeling of fundamental biomolecular circuits," *IEEE Trans. Biomed. Circuits Syst.*, 2015, IEEE Xplore website, Early Access.

[77] R. Sarpeshkar, "Analog versus digital: Extrapolating from electronics to neurobiology," *Neural Comput.*, vol. 10, pp. 1601–1638, 1998.

[78] S. S. Woo and R. Sarpeshkar, "A spiking-neuron collective analog adder with scalable precision," in *Proc. IEEE Int. Symp. Circuits and Systems*, Beijing, China, May 2013, pp. 1620–1623.

[79] S. Mandal, S. Zhak, and R. Sarpeshkar, "A bio-inspired active radio-frequency silicon cochlea," *IEEE J. Solid-State Circuits*, vol. 44, no. 6, pp. 1814–1828, Jun. 2009.

[80] J.-J. Sit and R. Sarpeshkar, "A cochlear-implant processor for encoding music and lowering stimulation power," *IEEE Pervasive Comput.*, vol. 1, no. 7, pp. 40–48, Jan.–Mar. 2008.

[81] H. Yang and R. Sarpeshkar, "A bio-inspired ultra-energy-efficient analog-to-digital converter for biomedical applications," *IEEE Trans. Circuits Syst. I, Reg. Papers*, vol. 53, no. 11, pp. 2349–2356, Nov. 2006.

[82] R. Sarpeshkar, "Brain power: Borrowing from biology makes for low-power computing," *IEEE Spectr.*, vol. 43, no. 5, pp. 24–29, May 2006, invited paper.

[83] L. Turicchia and R. Sarpeshkar, "A bio-inspired companding strategy for spectral enhancement," *IEEE Trans. Speech Audio Process.*, vol. 13, no. 2, pp. 243–253, Mar. 2005.

[84] R. Sarpeshkar and M. O'Halloran, "Scalable hybrid computation with spikes," *Neural Comput.*, vol. 14, no. 9, pp. 2003–2024, Sep. 2002.

[85] R. Hahnloser, R. Sarpeshkar, M. Mahowald, R. Douglas, and S. Seung, "Digital selection and analogue amplification coexist in a cortex-inspired silicon circuit," *Nature*, vol. 405, pp. 947–951, Jun. 22, 2000.

[86] R. Sarpeshkar, "Universal principles for ultra low power and energy efficient design," *IEEE Trans. Circuits Syst. II, Exp. Briefs*, vol. 59, no. 4, pp. 193–198, 2012.

[87] R. Sarpeshkar, R. F. Lyon, and C. A. Mead, "A low-power wide-dynamic-range analog VLSI cochlea," *Analog Integr. Circuits Signal Process.* , vol. 16, no. 3, pp. 245–274, Aug. 1998.
[88] R. Sarpeshkar, J. Kramer, G. Indiveri, and C. Koch, "Analog VLSI architectures for motion processing: From fundamental limits to system applications," *Proc. IEEE*, vol. 84, no. 7, pp. 969–987, 1996, Invited Paper.
[89] J. Bohorquez, W. Sanchez, L. Turicchia, and R. Sarpeshkar, "An integrated-circuit switched-capacitor model and implementation of the heart," in *Proc. 1st Int. Symp. Applied Sciences in Biomedical and Communication Technologies*, Aalborg, Denmark, Oct. 25–28, 2008, pp. 1–5, invited paper.
[90] U. Alon*, An Introduction to Systems Biology: Design Principles of Biological Circuits*. Boca Raton, FL, USA: Chapman & Hall/CRC, 2007.
[91] H. M. Sauro and K. Kim, "Synthetic biology: It's an analog world," *Nature*, vol. 497, no. 7451, pp. 572–573, 2013.
[92] Z. Z. Sun, E. Yeung, C. A. Hayes, V. Noireaux, and R. M. Murray, "Linear DNA for rapid prototyping of synthetic biological circuits in an escherichia coli based TX-TL cell-free system," *ACS Synth. Biol.*, vol. 3, no. 6, pp. 387–397, Jun. 2014.

Jonathan Teo received the B.A. degree in physics and biophysics from Johns Hopkins University, Baltimore, MD, USA, in 2012.

Currently, he is working toward the Ph.D. degree in computational and systems biology at the Massachusetts Institute of Technology, Cambridge, MA, USA. He is a graduate student in the Analog Circuits and Biological Systems group. His research interests include developing a deep quantitative understanding of biological systems in general. He is currently working on applying analog feedback control theory to biological circuit design and analysis, with a focus on stem cell homeostasis and the immune system.

Sung Sik Woo (S'10) received the B.S. degree (summa cum laude) in electrical engineering from the Korea Advanced Institute of Science and Technology (KAIST), Daejeon, Korea, and the M.S. degree in electrical engineering and computer science from the Massachusetts Institute of Technology (MIT), Cambridge, MA, USA, in 2009 and 2012, respectively.

Currently, he is working toward the Ph.D. degree in the Analog Circuits and Biological Systems Group at MIT. His research interests include the design and implementation of cytomorphic chips for synthetic and systems biology and bio-inspired collective analog computation.

Rahul Sarpeshkar received B.S. degrees in electrical engineering and physics from the Massachusetts Institute of Technology (MIT), Cambridge, MA, USA, and the Ph.D. degree from the California Institute of Technology, Pasadena, CA, USA.

Currently, he is the Thomas E. Kurtz Professor at Dartmouth College, Hanover, NH, USA, where he is also a Professor in the departments of Engineering, Physics, Microbiology and Immunology, and Physiology and Neurobiology. His research creates novel wet DNA-protein circuits in living cells and also advanced dry nano-electronic circuits on silicon chips. His longstanding work on analog and biological computation and his most recent work have helped pioneer the field of analog synthetic biology. His work on a glucose fuel cell for medical implants was featured by Scientific American among 2012's 10 World Changing Ideas. He holds over 35 awarded patents and has authored more than 125 publications, including one that was featured on the cover of Nature. His book *Ultra Low Power Bioelectronics: Fundamentals, Biomedical Applications, and Bio-Inspired Systems* revealed the deep connections between analog transistor circuits and biochemical circuits and founded the field of cytomorphic systems. His group holds several first or best records in analog, bio-inspired, synthetic biology, medical device, ultra low power, and energy harvesting systems. His work has applications in implantable medical devices for the deaf, blind, and paralyzed and in biotechnology and medical applications that benefit from cellular engineering. Before he joined Dartmouth's faculty, he was a tenured professor at MIT, leading the analog circuits and biological systems group at the Research Lab of Electronics. Before joining MIT, he was a member of the technical staff of Bell Labs' division of biological computation in their physics department.

Dr. Sarpeshkar has received several awards including the NSF Career Award, the ONR Young Investigator Award, and the Packard Fellows Award.